The role of binocular disparity in the neural representation of multiple moving stimuli in the visual cortex

Anjani Sreeprada Chakrala*, Jianbo Xiao*, Xin Huang

Department of Neuroscience, School of Medicine and Public Health,
University of Wisconsin – Madison

* These authors contributed equally to this work.

Correspondence should be addressed to:

Xin Huang, Department of Neuroscience, University of Wisconsin, Madison, WI 53705, USA
Email: Xin.Huang@wisc.edu

Keywords: neural encoding, binocular disparity, transparent motion, divisive normalization, segmentation, figure-ground segregation, natural scenes, object-based attention, extrastriate cortex

Acknowledgment

We thank Dr. Greg DeAngelis for sharing the data set of the disparity tuning curves of a large number of MT neurons from his lab to be used in our model, Bryce Arseneau for animal training, and Drs. Jennifer Coonen and Kevin Brunner at the Wisconsin National Primate Research Center for excellent veterinary care and surgical assistance.

Grant support

This research was supported by National Eye Institute Grant R01 EY022443.

Conflict of Interest

None.

Abstract

A fundamental process of vision is to segment visual scenes into distinct objects and surfaces. Stereoscopic depth and visual motion cues are particularly important for segmentation. However, how the primate visual system uses depth and motion cues to segment multiple surfaces in 3-dimensional space is not well understood. We investigated how neurons in the middle temporal (MT) cortex represented two overlapping surfaces located at different depths and moved simultaneously in different directions. We recorded neuronal activities in MT of three male macaque monkeys while they performed discrimination tasks under different attention conditions. We found that neuronal responses to overlapping surfaces showed a robust bias toward the horizontal disparity of one of the two surfaces. For all animals, the disparity bias in response to two surfaces was positively correlated with the disparity preference of the neurons to single surfaces. For two animals, neurons that preferred the near disparities of single surfaces (near neurons) showed a near bias to overlapping stimuli, and neurons that preferred the far disparities (far neurons) showed a far bias. For the third animal, both near and far neurons showed a near bias, although the near neurons showed a stronger near bias than the far neurons. Interestingly, for all three animals, both near and far neurons showed an initial near bias relative to the average of the responses to the individual surfaces. Although attention can modulate neuronal response to better represent the attended surface, the disparity bias was still present when attention was directed away from the visual stimuli, indicating that the disparity bias cannot be explained by an attention bias. We also found that the effect of attention modulation of MT responses was consistent with object-based rather than feature-based attention. We proposed a model in which the pool size of the neuron population that weighs the responses to individual stimulus components can be variable. Our model is a novel extension of the standard normalization model and provides a unified explanation of the disparity bias across animals. Our results revealed the neural encoding rule for multiple moving stimuli located at different depths and showed new evidence of response modulation by object-based attention in MT. The disparity bias would allow subgroups of neurons to preferentially represent individual surfaces at different depths of multiple stimuli and therefore facilitate segmentation. Attention can further select a surface and enhance its neural representation.

Introduction

Natural scenes often contain multiple objects and surfaces in 3-dimensional space. Segmenting scenes into distinct objects and surfaces is fundamental to primate vision. Among visual features, stereoscopic depth and motion velocity are important cues aiding segmentation. While depth (Wallace and Mamassian 2004) or motion cue alone (Wallace and Mamassian 2003) can lead to segmentation, when combined they further enhance segmentation (Snowden and Rossiter 1999; Goutcher 2016; Kohler et al. 2019; Nawrot and Blake 1989; Bradshaw and Rogers 1996; Ban et al. 2012). For example, psychophysical studies have shown that it becomes easier to segment overlapping surfaces moving in different directions when they are located at different depths than at the same depth (Hibbard and Bradshaw 1999; Greenwood and Edwards 2006).

Although the neural representation of the horizontal disparity of a single stimulus in the visual cortex has been well characterized (Cumming and Parker, 1999; Prince et al. 2002; DeAngelis and Uka 2003), how the visual system represents multiple horizontal disparities of visual stimuli located at different depths is poorly understood. Previous neurophysiology studies have characterized how neurons in V1 and the middle-temporal (MT) cortex represent multiple motion directions of overlapping stimuli located at the same depth (Snowden et al. 1991; Qian and Andersen, 1994; Treue et al. 2000; Krekelberg and van Wezel, 2013; Xiao et al. 2014; McDonald et al. 2014; Xiao and Huang 2015; Wiesner et al 2020). Relatively little is known about the neural representation of multiple stimuli moving at different depths. In one study, Bradley and colleagues (1995) showed that the responses of MT neurons became stronger as the difference between the horizontal disparities of two overlapping stimuli moving in opposite directions increased. This suggests that increasing the disparity difference between two surfaces reduces inhibition between motion signals. However, this study investigated the interaction between motion and disparity cues only for the preferred and null directions of each neuron. To fully understand the neural representation of multiple moving stimuli and the impact of depth cues, it remains to be determined how neurons respond to a full range of motion directions and how depth cues influence the direction tuning to multiple moving stimuli. In response to a single stimulus, MT neurons encode motion direction and disparity independently such that the response tuning for a single motion direction does not change its shape as the disparity of the moving stimulus is varied (Smolyanskaya et al. 2013). It is still unclear how the disparities of multiple stimuli influence the response tuning to multiple motion directions.

Attention can bias neuronal responses elicited by multiple 2-dimensional stimuli in the receptive field (RF) in favor of the attended stimulus (Desimone and Duncan, 1995; Reynolds et al., 1999; Li and Basso, 2005; Treue and Maunsell, 1996; Ferrera and Lisberger, 1997; Treue and Martinez-Trijillo, 1999; Recanzone and Wurtz, 2000; Wannig et al., 2007). The effects of selective attention on the neural representation of multiple moving stimuli located at different depths remain to be determined.

We investigated the roles of horizontal disparity and attention in the neural representation of multiple stimuli moving in different directions. We characterized how neurons in area MT of macaque monkeys represented two overlapping surfaces located at different disparities and moved in different directions. Area MT is known for its importance in motion and depth perception and MT neurons are tuned to both motion direction in the frontoparallel plane and horizontal disparity (Maunsell and Van Essen, 1983a, 1983b; Bradley et al. 1995; DeAngelis and Newsome 1999;

DeAngelis and Uka 2003). We recorded the activities of MT neurons while two animals performed a novel direction-discrimination task and reported the motion direction of a cued surface of two overlapping stimuli located at different disparities. We also recorded neural activity while a third animal performed a discrimination task with attention directed away from the RFs. We characterized the full direction tuning curves of MT neurons to multiple motion directions at different disparities, as we manipulated the angular separation of two motion directions and the attention. We tested the hypothesis that disparity cues bias the direction-tuning curves of MT neurons to preferentially represent one surface of overlapping stimuli and therefore facilitate segmentation. We further hypothesized that such disparity bias can be modulated by attention but was not caused by attention. We found that MT responses to overlapping stimuli showed a robust bias toward the horizontal disparity of one of two surfaces, and the disparity bias can be modulated but not dependent on attention. We also showed new evidence of response modulation by object-based attention in MT. We proposed a model in which the pool size of the neuron population that weighs the responses to individual stimulus components can be variable. The model together with divisive normalization provides a unified explanation of our finding of the disparity bias and the individual differences across animals.

Results

We asked how the visual system utilizes motion and stereoscopic depth cues jointly to segment multiple visual stimuli. For this, we characterized how neurons in the middle-temporal (MT) cortex of macaque monkeys represent overlapping stimuli that were located at different depths and moving in different directions, while monkeys performed a direction discrimination task.

Behavioral task and performance

We trained two male macaque monkeys (B and G) to perform a direction discrimination task (see Methods). Visual stimuli were two overlapping random-dot surfaces moving simultaneously in two different directions at two depths of -0.1° (near) and 0.1° (far) horizontal disparity. The two motion directions were separated by either 60° or 120° and the vector average (VA) direction was varied randomly across 360° in a step of 30°. The monkey's task was to report the motion direction of the surface at a cued depth (either near or far) by making a saccadic eye movement to one of twelve reporting targets (a 12 AFC task) (Fig. 1A, B). To perform the task well, the monkeys must segment two overlapping surfaces and identify the direction of the cued surface. We randomly interleaved the experimental trials in which either the near surface (Fig. 1A) or the far surface (Fig. 1B) was cued. We referred to these trials as "Attend Near" and "Attend Far" trials, respectively. Also randomly interleaved were trials in which only a single surface was presented at either the near (-0.1°) or far (0.1°) disparity ("Single Near" and "Single Far"). Our data set included 49 behavior and neural recording sessions from monkey B, and 44 sessions from monkey G. Across the single- and two-surface trials, monkey B performed at a mean correct rate of 75% (STD = 6.6) (single-surface 87%, two-surface 72%), and monkey G performed at 72% correct (STD = 8.1) (single-surface 87%, two-surface 68%). As expected, both monkeys performed significantly better in the single-surface trials than in the two-surface trials (signed rank test, $p < 10^{-8}$). Notably, while monkey B performed equally well in the "Attend Near" and "Attend

Far" trials of overlapping stimuli (signed rank test, p = 0.56) (Fig. 1C, D), monkey G performed significantly better at discriminating the motion direction of the near-surface (mean correct rate 72%) than the far-surface (mean correct rate 65%) of overlapping stimuli (signed rank test, p= 4.3×10^{-13}) (Fig. 1E, F).

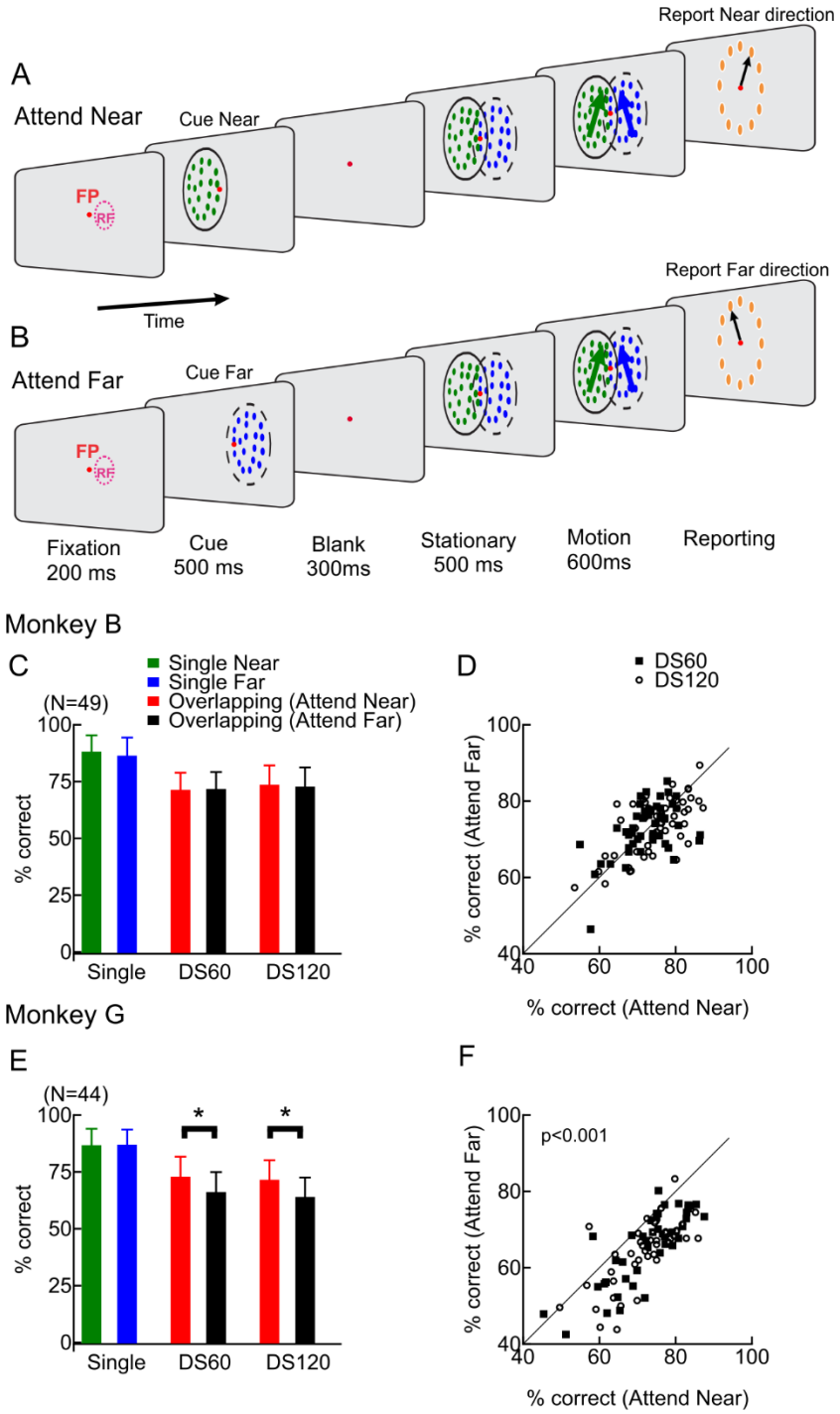

Figure 1. Discrimination task and behavioral performance.

A, B. Each trial started with the fixation on a target at the center of the monitor, then a stationary random dot patch (RDP) was presented for 500 ms at either -0.1° (near) disparity (A) or 0.1° (far) disparity (B) randomly as a cue. After 300 ms blank period, either two overlapping RDPs- one at near and one at far disparity ("Attend Near" and "Attend Far" trials as shown in (A) and (B)) or a single RDP ("Single Near" and "Single Far" trials not shown in the figure) appeared stationary for 500 ms, and then moved for 600ms. At the end of each trial, the monkey made an eye movement to report the motion direction of the RDP at the cued (Near or Far) disparity to receive a juice reward. **C.** Average % of correct choice trials across 49 recording sessions of Monkey B for Single (green: "Single Near", blue: "Single Far") and Overlapping motion directions (red: "Attend Near", black: "Attend Far"). DS60 and DS120 indicate 60° and 120° separations between overlapping motion directions. The error bars show standard deviations. **D.** % of correct choice trials of "Attend Near" conditions (or Cue Near) and "Attend Far" (or Cue Far) conditions are plotted on the x and y axes, respectively. Each symbol represents one recording session. Solid squares and open circles are for DS60 and DS120 conditions. **E.** Same as **C** for Monkey G across 44 sessions. (*) indicates $p<0.001$, paired signed rank test. **F.** Same as **D** for Monkey G. p-value is from one-sided signed rank test comparing x and y values.

Direction tuning curves of example neurons to overlapping stimuli moving at different depths.

Figure 2 shows the direction tuning curves (red and black) of four example MT neurons to overlapping stimuli moving in different directions at different depths, referred to as the "bi-directional stimuli". The direction tuning curves to the constituent near-surface and far-surface when they were presented alone, referred to as the "near component" and "far component" were shown in green and blue, respectively. If a neuron's maximum response of the directing tuning curve to the near component was greater than that to the far component, we classified the neuron as near-preferred ("near neuron" in brief), and vice versa as far-preferred ("far neuron").

Figures 2A1-D1 and 2A2-D2 show the responses of a near neuron and a far neuron from monkey B, elicited by the stimuli shown in Fig 2A-D (single component stimuli not shown in the illustration). The response tuning curve to the bi-directional stimuli of the near example neuron (red curve) showed a clear bias toward the tuning curve to the near component (green curve) when the monkey attended to the near surface (Fig. 2A1-D1). We referred to this response bias as a "near bias". The near neuron responded more strongly to the near than the far component, and therefore the average of the responses to the near and far components (gray dashed line) had a peak toward the near component. However, the red curve showed more bias toward the near component than expected by averaging the component responses (Fig. 2A1-D1). This near bias was found at both angular separations of 60° (Fig. 2A1, B1) and 120° (Fig. 2C1, D1). The near bias was also found regardless of whether the motion direction of the near component was at the clockwise (Fig. 2A1, C1) or counterclockwise side (Fig. 2B1, D1) of the two motion directions, suggesting that this bias was not toward a specific direction component. When monkey B attended to the far surface, the response to the bi-directional stimuli of the near neuron (black curve) still showed a near bias in some stimulus conditions (Fig. 2A1, C1, D1), but to a lesser degree than when the monkey attended to the near surface. In contrast, the far example neuron showed a clear bias (black curve) toward the far component when monkey B attended to the far surface (Fig. 2A2-D2). When the monkey attended to the near surface (red curve), the far bias was still clearly present in some conditions (Fig. 2C2, D2) but was weaker than when the monkey attended to the far surface. We also noticed that, in addition to the preference for one of the two binocular disparities, some neurons preferred one of the two motion directions as previously reported by Xiao and Huang (2015) using two-

dimensional stimuli. For example, the far neuron in Figure 2A2-D2 showed a stronger far bias when the far component was at the counterclockwise side (Fig. 2A2) than at the clockwise side of the two motion directions (Fig. 2B2). Our experimental design allowed us to separate the effect of disparity bias from the directional bias as shown below.

Figures 2A3-D3 and 2A4-D4 show the responses of a near neuron and a far neuron from monkey G. Remarkably, regardless of whether a neuron was near- or far-preferred and whether monkey G attended to the near or far surface, the responses to the bi-directional stimuli (red and black curves) showed a clear bias toward the near component. The responses to the bi-directional stimuli of these two neurons also showed little difference between the attending near and far conditions (comparing the red and black curves).

Population-averaged tuning curves to bi-directional stimuli moving at different depths

The results shown in the example neurons were representative across populations of neurons for monkeys B and G. Figure 3 shows the tuning curves to bi-directional stimuli averaged across near neurons and far neurons, at 60° and 120° angular separation. The direction tuning curve of each neuron was first fitted with a spline, normalized, and then shifted such that the vector average (VA) direction 0° of the bi-directional stimuli was aligned with the neuron's preferred direction (see Methods). The spline-fitted tuning curves were then averaged across near neurons and far neurons. To balance the potential bias toward one of two motion directions, we averaged the response tuning curves to bi-directional stimuli when the near component was at the clockwise side (Near C-Far CC in Fig 2) and counterclockwise side of the two motion directions (Near CC-Far C). To do so, before averaging we flipped the tuning curves relative to VA 0° when the near component was at the counterclockwise side of the two motion directions to the clockwise side (see Methods). As a result, in Figure 3 the near component is always at the "clockwise" side of the two motion directions.

For monkey B, population-averaged tuning curves to bi-directional stimuli showed a clear bias toward neurons' preferred disparity, i.e., near neurons showed a bias toward the near component (Fig. 3A, C), whereas far neurons showed a bias toward the far component (Fig. 3B, D). The disparity bias was modulated by attention – near neurons showed a stronger near bias when monkey B attended to the near surface (Fig. 3A, C) and far neurons showed a stronger far bias when monkey B attended to the far surface (Fig. 3B, D). Nevertheless, the disparity bias cannot be explained by attention modulation. For example, far neurons still showed a clear far bias even when monkey B attended to the near surface (red curve in Fig. 3D).

In contrast, for monkey G, population-averaged tuning curves to bi-directional stimuli showed a robust bias toward the near component for both near neurons (Fig. 3E, G) and far neurons (Fig. 3F, H), and in trials when either the near or the far surface was cued for attention. We found very small attention modulation, if any, in the data from monkey G.

As an attention control, we asked whether MT neurons showed disparity biases without the involvement of attention. To do so, we trained a third monkey R to perform a fine direction discrimination task in the visual hemifield opposite from the RFs, while we presented the bi-directional stimuli and individual stimulus components in the RFs (see Methods). The results from

monkey R showed a similar disparity bias as found in monkey B – near neurons tended to show a near bias (Fig. 3I, K) and far neurons tended to show a far bias (Fig. J, L). In other words, a neuron's response to bi-directional stimuli tends to show a bias toward the stimulus component located at the neuron's preferred disparity.

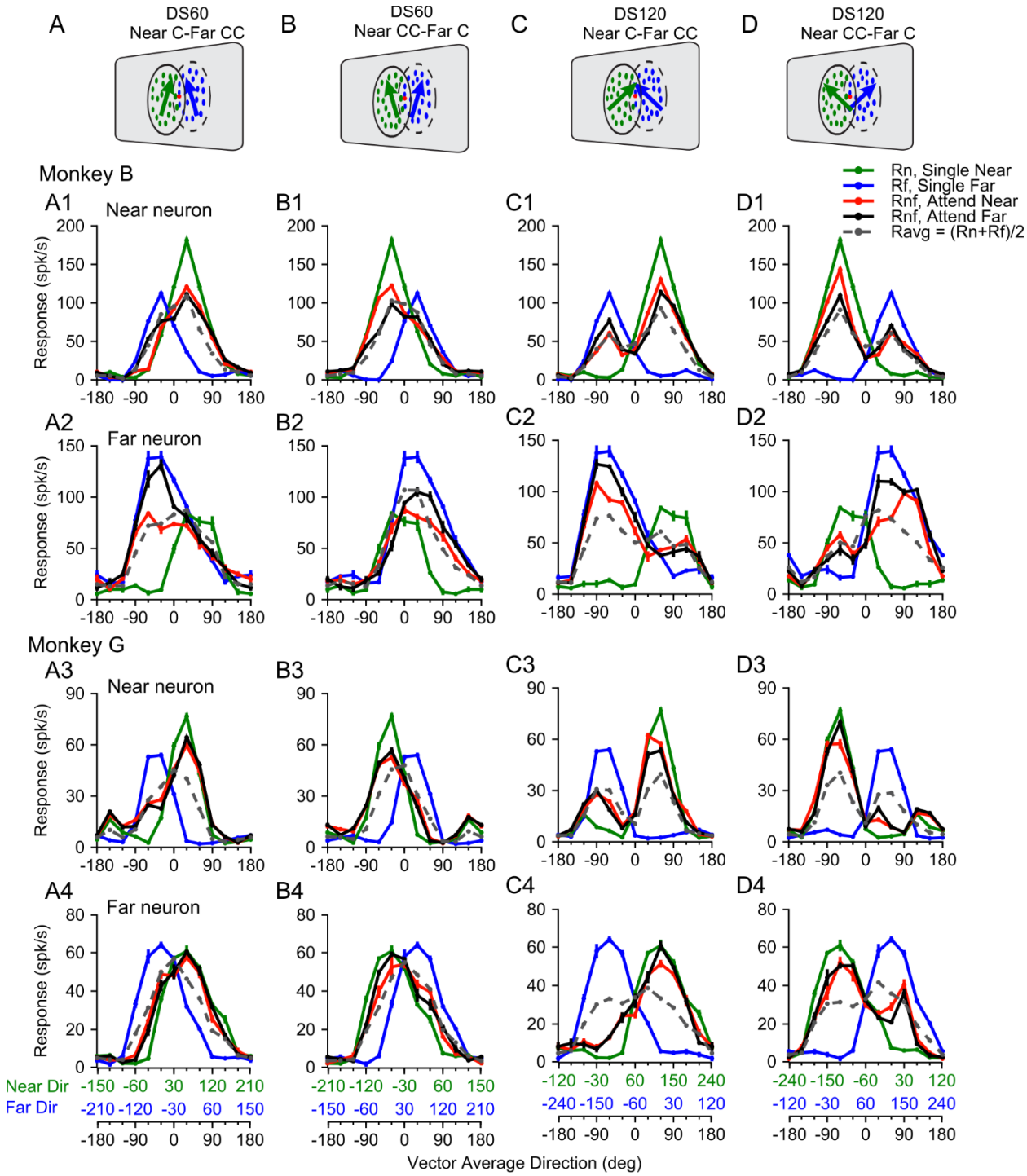

Figure 2. Example MT neurons' tuning curves to single and overlapping stimuli moving at different depths.

A-D. Schematic showing overlapping stimuli used in the discrimination task. Two RDPs (near and far surfaces in green and blue, respectively) moved in different directions such that their angle separation is either 60° or 120° (DS60 and DS120) with different angular arrangements: near motion direction on clockwise side and far motion direction on counterclockwise side (Near C-Far CC) and vice-versa (Near CC-Far C). Colors were used for illustrative purposes only. **A1-A4, B1-B4, C1-C4, D1-D4** are response tuning curves of example neurons to the stimuli shown in **A, B, C, D**, respectively, with the vector average direction (VA) of the two directions varied across 360° at a 30° step. **A1-D1.** Tuning curves of an example near neuron of monkey B to overlapping (bi-directional) stimuli (red: Attend Near and black: Attend Far conditions) and the single component directions (green: Single Near and blue: Single Far). Grey dashed lines show the average of the single component direction tuning curves (green and blue). **A2-D2.** Direction tuning curves of an example far neuron of Monkey B. **A3-D3.** Direction tuning curves of an example near neuron of Monkey G. **A4-D4.** Direction tuning curves of an example far neuron of Monkey G. The x-axes in green and blue show single near and far direction components, respectively, of the corresponding bidirectional stimuli for which the vector average (VA) direction is shown by the x-axis in black. A VA direction of 0° is aligned with the neuron's preferred direction (PD).

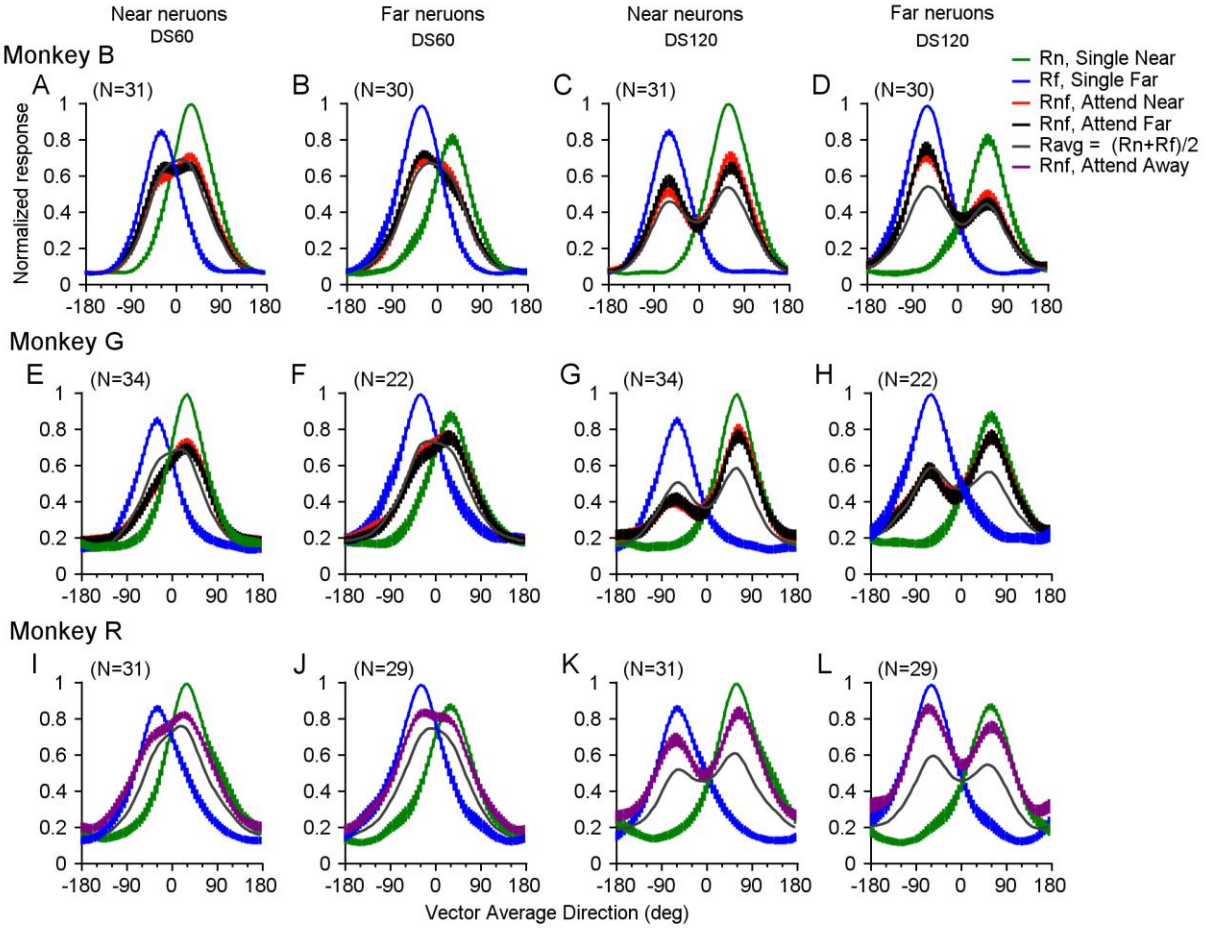

Figure 3. Population-averaged tuning curves to single and overlapping stimuli moving at different depths.

A, E, I. Tuning curves to bidirectional stimuli with 60° direction separation (DS60) averaged across all near neurons. **B, F, J.** Averaged across all far neurons. **C, G, K.** Tuning curves to bidirectional stimuli with 120° direction separation (DS120) averaged across all near neurons. **D, H, L.** Averaged across all far neurons. **A-D.** Monkey B. **E-H.** Monkey G. **I-L.** Monkey R from the Attend away paradigm. The width of

each curve indicates standard error. For each panel, Near CC-Far C tuning curves (like in Fig 2) were spline-fitted, normalized, and flipped along the x-axis (-180° to 180° VA) and were averaged with Near C-Far CC spline-fitted, normalized tuning curves across near or far neurons.

Response bias toward the near or far component and effect of attention

To quantify the response biases toward either the near or far component, we fitted the bi-directional tuning curves of each neuron (red and black curves as in Fig 2) as a weighted sum of the responses to the individual stimulus components (green and blue curves as in Fig 2). We found that a model of weighted summation plus a nonlinear interaction term (Eq. 1), referred to as the SNL model, provided a significantly better fit than a linear weighted summation (LWS) model shown in Eq. 13 (Supplementary Fig. 1, one-sided signed rank test, $p < 10^{-7}$, SNL model mean PV Monkey B =93%, Monkey G =83%, Monkey R =88%; LWS model mean PV: Monkey B PV =91%, Monkey G PV =81%, Monkey R PV =82%, see Eq.16 for PV).

$$R_{pred}(\theta_n, \theta_f) = w_n R_n(\theta_n) + w_f R_f(\theta_f) + b R_n(\theta_n) R_f(\theta_f) \qquad (1)$$

in which R_{pred} is the model-predicted response to bi-directional stimuli moving in directions θ_n and θ_f; R_n and R_f are the direction tuning curve to single motion directions at the near and far surface, respectively; w_n and w_f are two model parameters and represent the response weights for the near and far component, respectively; b is a third model parameter that determines the strength and sign of a multiplicative interaction between two component responses.

We defined a weight bias index (*WBI*) as: $WBI = (w_n - w_f)/(w_n + w_f)$. A positive *WBI* indicates a bias toward the near component, whereas a negative *WBI* indicates a bias toward the far component. Figure 4 shows the distributions of *WBI* across near and far neurons and the effect of attention. In the scatter plots (Fig. 4A, B), each neuron contributed to four data points, for 60° and 120° angular separation and the near component moving at either the clockwise or counterclockwise side of two motion directions, respectively. For monkey B, near neurons had significantly larger *WBI* than the far neurons regardless of whether the monkey attended to the near or far surface (one sided sign rank test, $p < 0.001$) (Fig. 4A). When the monkey attended to the near surface, near neurons showed a significant near bias (mean *WBI* = 0.12, p= 1.4310e-08, one sided sign rank test comparing mean to zero), and far neurons showed a significant far bias (mean *WBI* = -0.17, p= 1.9459e-08). When the monkey attended to the far surface, far neurons showed a significant far bias (mean *WBI* = -0.30, p= 5.7378e-15), and near neurons had a mean *WBI* of -0.01 which was not different from zero (p = 0.0537). Attention had a significant effect on *WBI*, giving rise to a larger *WBI* when monkey B attended to the near surface than the far surface across near neurons ($p = 5.4 \times 10^{-9}$), far neurons (p = 0.007), and all neurons combined (p= 3.0086e-10) (Fig. 4A).

For monkey G, however, both near and far neurons showed a significant near bias, regardless of whether the near surface or the far surface was cued for attention (p= 6.0931e-56). Furthermore, attention did not change *WBI* significantly across the near neurons (p = 0.29), far neurons (p = 0.59), and all neurons combined (p = 0.41). Nevertheless, near neurons still showed a significantly larger *WBI* than the far neurons when monkey G attended to the near surface (p <

0.01) and when the attending near and attending far conditions were pooled (one-sided rank sum test, p=0.002).

For monkey R, we found a similar result that the near neurons showed a significantly larger *WBI* than the far neurons when monkey R attended away from the RFs (p= 3.9412e-05) (Fig. 4C). Near neurons showed a significant near bias (mean *WBI* = 0.07, p = 4.3×10^{-4}) and far neurons showed a significant far bias (mean *WBI* = -0.03, p = 0.003). In summary, MT neurons in monkeys B and R showed a significant bias toward the stimulus component moving at the neurons' preferred disparity. Although neurons in monkey G showed a predominant near bias, near neurons also tended to show a stronger near bias than the far neurons.

Relationship between disparity bias in responses to two surfaces and disparity preference to single surface

To quantify the disparity bias and to balance the effect of potential directional bias, we defined a two-surface disparity bias index (*TDBI*) that pooled the response weights obtained when the near component moved either in the clockwise (*nC*) or counterclockwise (*nCC*) direction of the two motion directions from Eq.1 :

$$TDBI = \frac{(w_n - w_f)_{nC} + (w_n - w_f)_{nCC}}{(w_n + w_f)_{nC} + (w_n + w_f)_{nCC}} \qquad (2)$$

A positive *TDBI* indicates a bias toward the near component of two overlapping stimuli and a negative *TDBI* indicates a bias toward the far component. We examined the relationship between the disparity bias to one of the components of overlapping stimuli and a neuron's preference for the disparity of a single surface, measured by a single surface disparity preference index (*SDPI*):

$$SDPI = \frac{\max(R_n) - \max(R_f)}{\max(R_n) + \max(R_f)} \qquad (3)$$

in which R_n and R_f *are* the direction tuning curves to the near and far surfaces when presented alone, as defined in Eq. 1. A positive and negative *SDPI* indicate a preference for the near and far disparity, respectively. Figure 5 shows that, for all three animals, the *TDBI* is significantly correlated with the *SDPI* ($p < 0.01$) (Pearson correlation coefficient r = 0.57, 0.31, and 0.24 for monkeys B, G, and R, respectively). The positive correlation was robust regardless of whether monkeys B and G attended to the near or far surface (Fig. 5A, B), or whether attention was directed away from the RF (Fig. 5C). For monkey G, even though most of the neurons showed a near bias and preferred near disparity, the positive correlation between *TDBI* and *SDPI* still holds, indicating a common trend across animals.

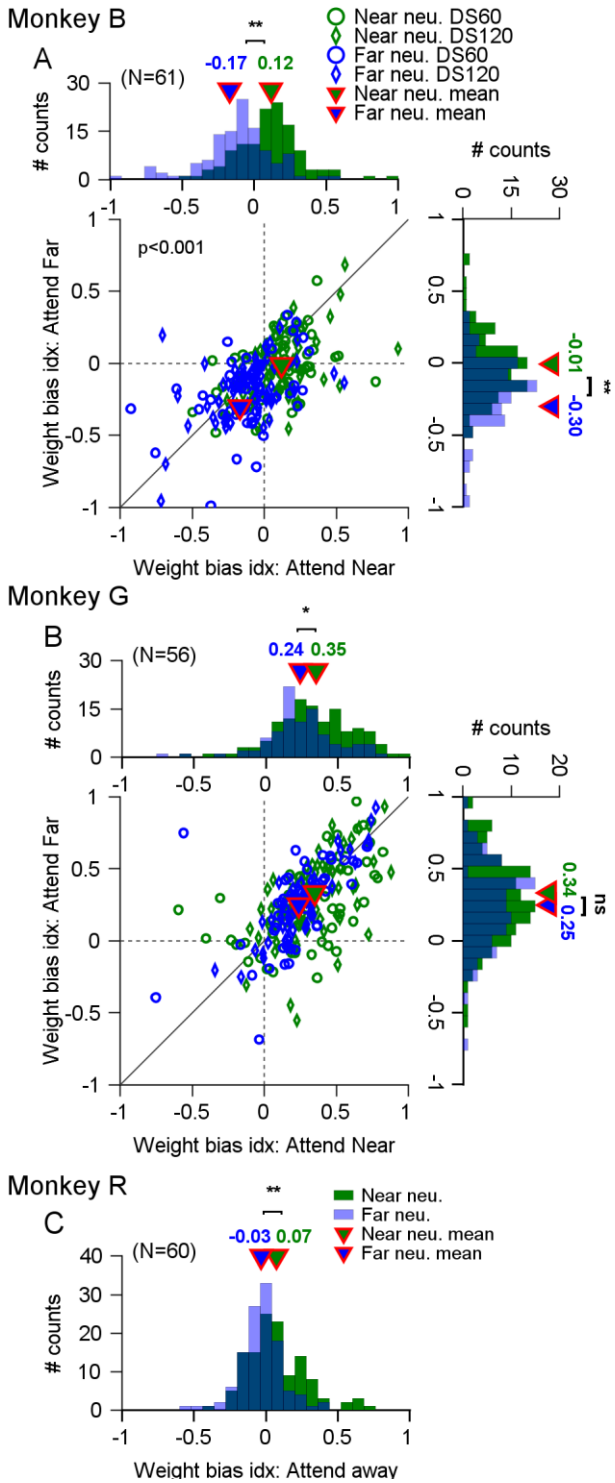

Figure 4. Effects of attention on the response weights of the near and far components.

A. Comparison of the weight bias indices (WBIs, $wbi = (w_n - w_f)/(w_n + w_f)$, Eq. 1) of Attend Near and Attend Far conditions, respectively from monkey B. Each dot represents the result from one bi-directional tuning curve of a neuron. Open circles and solid diamonds correspond to DS60 and DS120 conditions, respectively. Each neuron contributes to two of each of the symbols- one from Near C-Far CC and the other

from Near CC-Far C conditions. Green and blue dots denote near and far neurons. The triangles show the mean values for each group. p value in the scatter plot is of paired signed rank test. The histograms show the distributions of WBIs for the Attend Near (top) and Attend Far (right) conditions for near (green) and far (blue) neurons **B.** Same as **A** for monkey G. **C.** The histograms show the distributions of WBIs for the Attend away paradigm for near (green) and far (blue) neurons from monkey R. (**) indicates $p<0.001$, (*) indicates $p<0.01$, (ns) indicates $p>0.05$, one-sided signed rank test.

Time course of the response tuning to bi-directional stimuli moving at different depths

To understand the nature of disparity bias and the underlying mechanisms, we asked the following questions. First, did the disparity bias emerge at the beginning of the neural response or build up over time? Second, what was the relationship between the disparity bias and attention modulation? Third, did the neuronal population in MT show an overall bias to the near or the far disparity of two surfaces? To answer these questions, we characterized the time course of the response tuning curves to the bi-directional stimuli moving at different depths.

Figure 6 shows the population-averaged tuning curves of monkey B to the bi-directional stimuli, calculated within a sliding time window of 50 ms at a step of 10 ms. As in Figure 3, we combined the conditions in which the near component moved at either the clockwise or the counterclockwise side of the two directions (see Methods). In the combined responses, we plotted the near component at the clockwise side of the two motion directions. As such, at positive VA directions, the near component moved in a more preferred direction of the neurons and elicited a stronger response than the far component. Specifically, at the VA direction of 30º and 60º, the near component moved in the preferred direction (0º) of the neuron when the angular separation was 60º and 120º, respectively. We referred to VA 30º or 60º as "Near PD". Conversely, at negative VA directions, the far component moved in a more preferred direction and elicited a stronger response (Figs. 6A1-D1). At the VA direction of -30º and -60º, the far component moved in the preferred direction (0º) at the angular separation of 60º and 120º, respectively. We referred to VA -30º or -60º as "Far PD". When the response tuning to the bi-directional stimuli is biased toward the near component, the tuning curve should skew to the positive VA directions. Likewise, when the bias is toward the far component, the tuning should skew to the negative VA directions.

At 60º angular separation, the near neurons showed a slightly delayed near bias, starting about 40 ms after the response onset (Fig. 6A2, A3). Attending the near surface made the near bias strong and persistent over time (Fig. 6A2). Attending the far surface did not abolish the initial near bias, but later shifted the tuning back and forth between the near and far components and made the tuning broader than attending near (Fig. 6A3). Consistently, the far neurons showed a delayed far bias (Fig. 6B2, B3). Attending the far surface made the far bias more robust and persistent over time (Fig. 6B3) than attending near. Nevertheless, far neurons still showed clear far bias even when attention was directed to the near surface (Fig. 6B2). For both the near and far neurons, the average of the responses to the near and far components (Ravg) were roughly balanced over time around VA 0º, with a slight near (Fig. 6A4) and far (Fig. 6B4) skewness.

Similarly, at 120º angular separation, the near neurons showed a near bias (Fig. 6C2, C3) and the far neurons showed a far bias (Fig. 6D2, D3). The disparity bias appeared sooner than that at 60º angular separation. Selective attention modulated the responses but was not sufficient to change the disparity bias according to attention (Fig. 6C3, 6D2). For both the near and far neurons,

the Ravg was slightly skewed toward the neurons' preferred disparity during the early response (Fig. 6C4, 6D4).

To separate the disparity bias from the effect of selective attention, we averaged the tuning curves obtained from "Attend Near" and "Attend Far" conditions (Fig. 7A1-D1). We further examined the disparity bias as the deviation from the average of the component responses by subtracting Ravg from the attention-averaged responses (Fig. 7A2-D2). At both 60º and 120º angular separations, we found that the near neurons showed an earlier, initially stronger, and more transient near bias (Fig. 7A2, C2) than the far bias of the far neurons (Fig. 7B2, D2). Furthermore, the near bias at 60º angular separation was slightly delayed relative to that at 120º angular separation (comparing Fig. 7A2 with C2, and Fig. 7B2 with D2). At 60º angular separation, the disparity bias was reflected in response facilitation at the biased side, and suppression near VA 0º and the other side of the VA directions (Fig. 7A2, B2). At 120º angular separation, the disparity bias was reflected in stronger response facilitation on the biased side than on the other side (Fig. 7C2, D2). The suppression near VA 0º was stronger for the near neurons than the far neurons (comparing Fig. 7A2 vs B2, and 7C2 vs D2).

To examine the effects of selective attention, we subtracted the response of one attention condition from the other (Fig. 7A3-D3). For near neurons, the attention modulation was reflected in response facilitation at positive VA directions around "Near PD", and/or suppression at negative VA directions around "Far PD" (Fig. 7A3, C3). The facilitation (Fig. 7A3) and suppression (Fig. 7A3, C3) occurred as soon as the response onset. In contrast, for far neurons, the attention modulation was mainly reflected in much-delayed facilitation at negative VA directions around "Far PD" (Fig. 7B3, D3).

Figures 8 and 9 show the results from monkey G. The latency of the response to two surfaces in depths was about 30 ms delayed relative to that of monkey B (indicated by white dashed lines in Fig. 8A2), whereas the response latency to 2D stimuli showed no difference between the two animals (results not shown). At 60º angular separation, the near neurons of monkey G showed the development of near bias over a period of about 80 ms, starting from around 110 ms to fully biased to the near side around 190 ms (Fig. 8A2, A3; Fig. 9A1, 9A2). At 120º angular separation, the near neurons showed an earlier and stronger near bias than at 60º angular separation (Fig. 8C2, C3; Fig. 9C1, C2). The near bias was stronger and more persistent when attention was directed to the near surface (Fig. 8A2, C2) than to the far surface (Fig. 8A3, C3). Near neurons showed a small effect of attention modulation, mainly reflected in response facilitation at the positive VA directions around "near PD" when the response of attending far was subtracted from attending near (Fig. 9A3, C3). There was small initial facilitation toward negative VA directions around far PD at about 100 ms after motion onset (Fig. 9A3, C3), suggesting that the monkey may have initially attended the far surface briefly before attending the cued near surface.

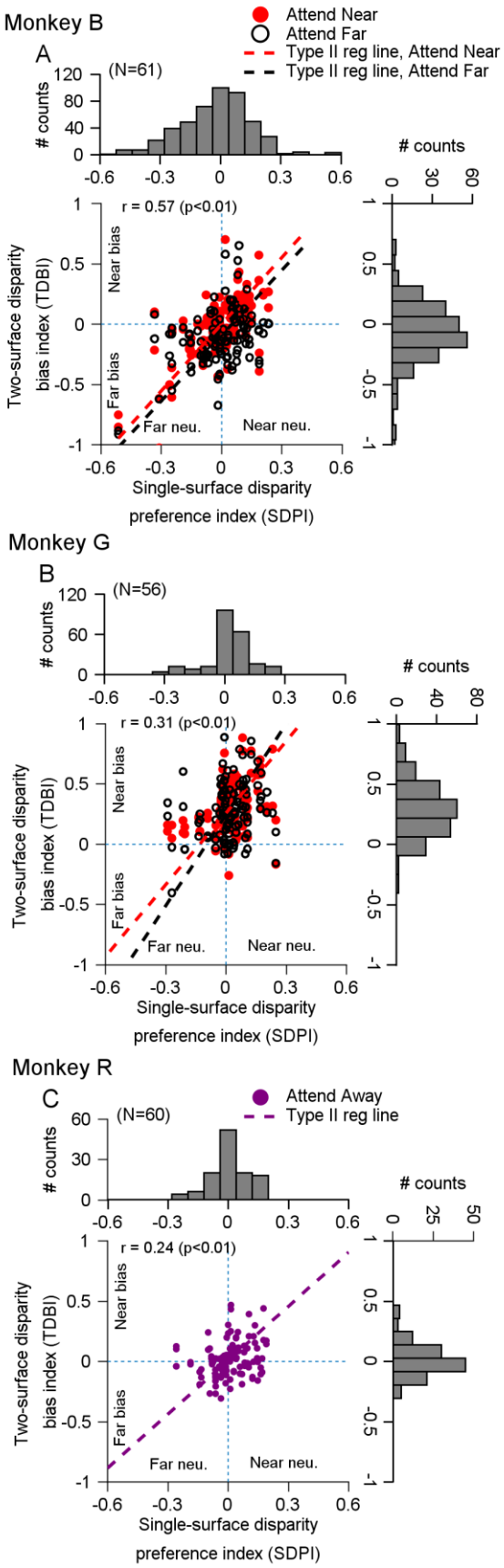
Monkey B
A
Attend Near
Attend Far
Type II reg line, Attend Near
Type II reg line, Attend Far
(N=61)
# counts
r = 0.57 (p<0.01)
Near bias
Far bias
Far neu.
Near neu.
Two-surface disparity bias index (TDBI)
Single-surface disparity preference index (SDPI)
Monkey G
B
(N=56)
r = 0.31 (p<0.01)
Monkey R
C
Attend Away
Type II reg line
(N=60)
r = 0.24 (p<0.01)

Figure 5. Relationship between MT neurons' response bias to the one of the two surfaces and their preference to single surfaces.

A. Comparison of Two-surface disparity bias indices (TDBIs) and Single-surface disparity preference indices (SDPIs) under Attend Near and Attend Far conditions, in red solid circles and black open circles, respectively from monkey B. Each neuron contributes to two symbols for each attention condition-one from DS60 and the other from DS120 conditions. The dotted lines are the type 2 regression fits. r is the Pearson correlation coefficient between x and y values of Attend Near and Attend Far (red and black symbols) together with the corresponding p values in brackets. The histograms show the distributions of TDBIs (top) and SDPIs (right). **B.** Same as **A** for monkey G. **C.** Same as **A** with Attend away paradigm from monkey R.

Remarkably, far neurons of monkey G also showed near bias (Fig. 8B2, B3, D2, D3; Fig. 9B1, D1) that had a similar time course as that of the near neurons (Fig. 9A2-D2). The responses of the far neurons to the bi-directional stimuli were robust and sustained at the positive VA directions around "near PD" throughout the motion period, making the tuning curve broader than the near neurons (comparing Fig. 9A1, B1). Far neurons showed little attention modulation at 60º angular separation (Fig. 9B3) and showed small and delayed facilitation at the negative VA directions around "far PD" at 120º angular separation when the response of attending near was subtracted from attending far (Fig. 9D3). Like near neurons, far neurons showed a small initial facilitation toward positive VA directions around near PD at about 100 ms (Fig. 9B3, D3), also suggesting that the monkey may have attended the other surface briefly before attending the cued surface. Regardless of the attention modulation, the near bias was robust throughout the motion response period.

When attention was directed away from the RF, the near and far neurons of monkey R showed disparity bias toward their preferred disparity roughly 50 ms after the response onset (Fig. 10). Within the early response period from 100 ms to 160 ms, the near bias of the near neurons was stronger than the far bias of the far neurons (Fig. 10A4-C4). For far neurons, the initial responses were roughly balanced between VA directions around the far PD and near PD and the far bias only became evident after 160 ms (Fig. 10B4, C4).

To address whether MT neurons showed an overall bias to the near or the far disparity of two surfaces, we pooled the results of near and far neurons for each animal and examined the time course of (RAttendNear + RAttendFar)/2 – Ravg for monkeys B and G, and RAttendAway – Ravg for monkey R (Fig. 11A1 to A3 and B1 to B3). To quantify the difference between the responses at the positive and negative VA directions, we flipped the responses at the negative VA directions relative to VA 0º and subtracted the flipped responses from the responses at the positive VA directions (Fig. 11C1 to C3 and D1 to D3). For all three animals, there was an initial near bias (marked by the horizontal dashed lines in Fig 11). For monkey B, the later response after 120 ms showed a net far bias (Fig. 11A1 to D1), whereas for monkey G, the near bias persisted in both earlier and later responses (Fig. 11A2 to D2). For monkey R, the later response was roughly balanced (Fig. 11A3 to D3). Taken together, the time course results showed that regardless of whether attention was engaged, the neural responses across three animals were initially biased toward the near surface of two overlapping stimuli.

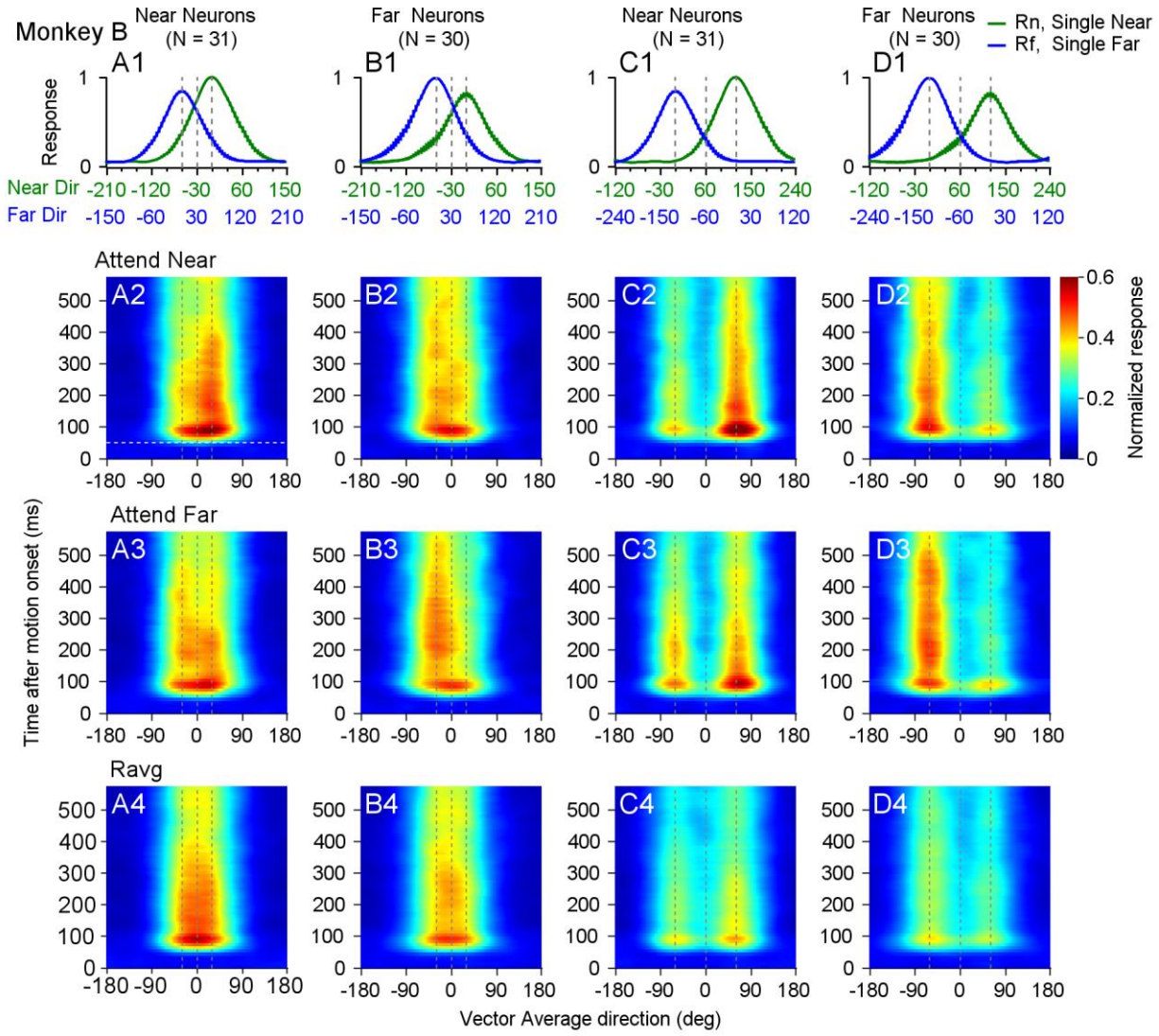

Figure 6. Time course of the response tuning to bi-directional stimuli moving at different depths in monkey B.

A1-D1. Responses to single component near and far directions. Motion directions and population averaged responses are plotted on x and y axes, respectively. The white dashed horizontal line in A2 indicates the response onset. **A2-D2.** Responses to bidirectional stimuli from "Attend Near" condition. Vector average (VA) direction of two motion directions, time after motion onset, and population averaged responses are plotted on x, y, and z axes, respectively. **A3-D3.** Responses to bidirectional stimuli from "Attend Far" condition. **A4-D4.** Responses to single component Near and Far directions in (A1 to D1) averaged together (R_{avg}). **A1-A4.** Averaged across near neurons for DS60 stimuli. **B1-B4.** Averaged across far neurons for DS60 stimuli. **C1-C4**. Averaged across near neurons for DS120 stimuli. **D1-D4.** Averaged across far neurons for DS120 stimuli. Vertical dashed lines in each panel indicate the responses to bidirectional stimuli with preferred direction at the near surface/less preferred direction at the far surface ("Near PD"), VA direction (x-axis) 0°, and preferred direction at the far surface/less preferred direction at the near surface ("Far PD") from right to left, respectively.

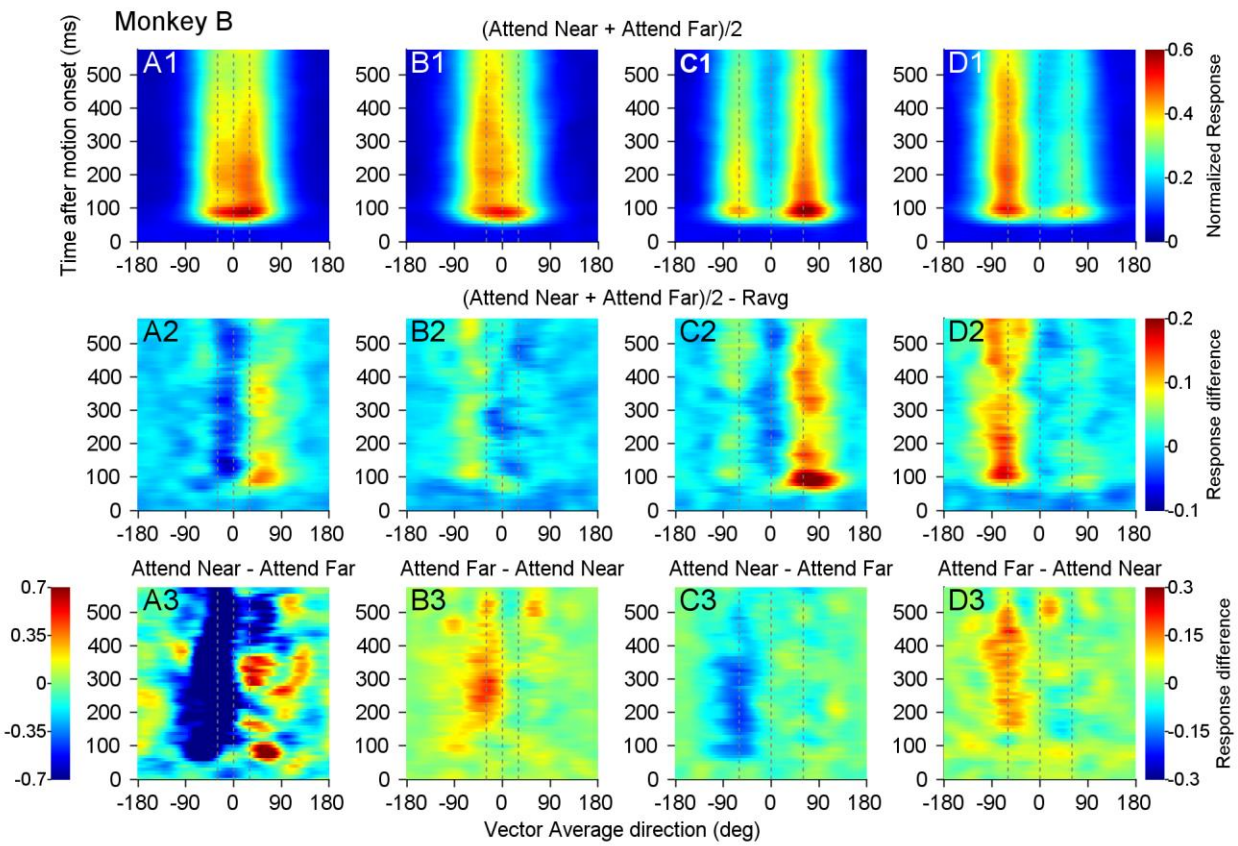

Figure 7. Temporal development of disparity bias and effects of selective attention in monkey B.

A1-D1. Responses to bidirectional stimuli in "Attend Near" (Fig 7 A2 to D2) and "Attend Far" (Fig 7 A3 to D3) conditions averaged together: $(R_{AttendNear} + R_{AttendFar})/2$. **A2-D2.** Difference between the responses from (Fig 7 A1 to D1) and (Fig 6 A4 to D4): $(R_{AttendNear} + R_{AttendFar})/2 - R_{avg}$. **A3, C3.** Difference between the responses from (Fig 6 A2, C2) and (Fig 6 A3, C3): $R_{AttendNear} - R_{AttendFar}$. **B3, D3.** Difference between the responses from (Fig 6 B3, D3) and (Fig 6 B2, D2): $R_{AttendFar} - R_{AttendNear}$. **A1-A3.** Averaged across near neurons for DS60 stimuli. **B1-B3.** Far neurons DS60. **C1-C3.** Near neurons DS120. **D1-D3.** Far neurons DS120. Vertical dashed lines in each panel indicate the responses to bidirectional stimuli with preferred direction at the near surface/less preferred direction at the far surface ("Near PD"), VA direction (x-axis) 0°, and preferred direction at the far surface/less preferred direction at the near surface ("Far PD") from right to left, respectively. Panels in each row have the same color bar scale shown on the right, except for A3 whose color bar is shown on the left of the panel.

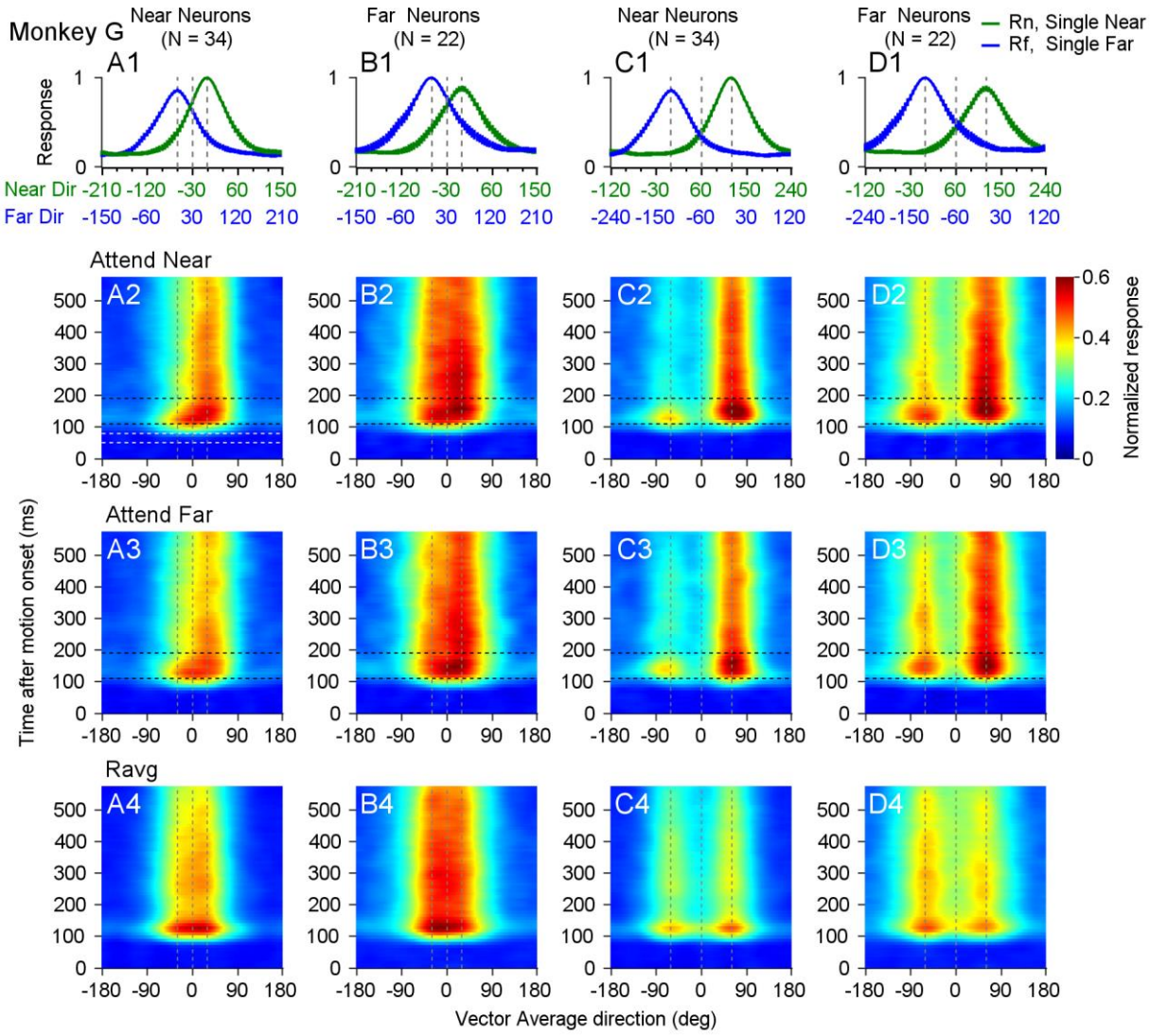

Figure 8. Time course of the response tuning bi-directional stimuli moving at different depths in monkey G.

A1-D1. Responses to single component near and far directions. Motion directions and population averaged responses are plotted on x and y axes, respectively. **A2-D2.** Responses to bidirectional stimuli from "Attend Near" condition. Vector average (VA) direction of two motion directions, time after motion onset, and population averaged responses are plotted on x, y, and z axes, respectively. The bottom and top white dashed lines in **A2** indicate the response onset of Monkey B and G, respectively, for comparison. **A3-D3.** Responses to bidirectional stimuli from "Attend Far" condition. The two black horizontal dashed lines in **A2-D2** and **A3-D3** mark the period of the development of near bias. **A4-D4.** Responses to single component near and far directions in (A1 to D1) averaged together (R_{avg}). **A1-A4.** Averaged across near neurons for DS60 stimuli. **B1-B4.** Averaged across far neurons for DS60 stimuli. **C1-C4.** Averaged across near neurons for DS120 stimuli. **D1-D4.** Averaged across far neurons for DS120 stimuli. Vertical dashed lines in each panel indicate the responses to bidirectional stimuli with preferred direction at the near surface/less preferred direction at the far surface ("Near PD"), VA direction (x-axis) 0°, and preferred direction at the far surface/less preferred direction at the near surface ("Far PD") from right to left, respectively.

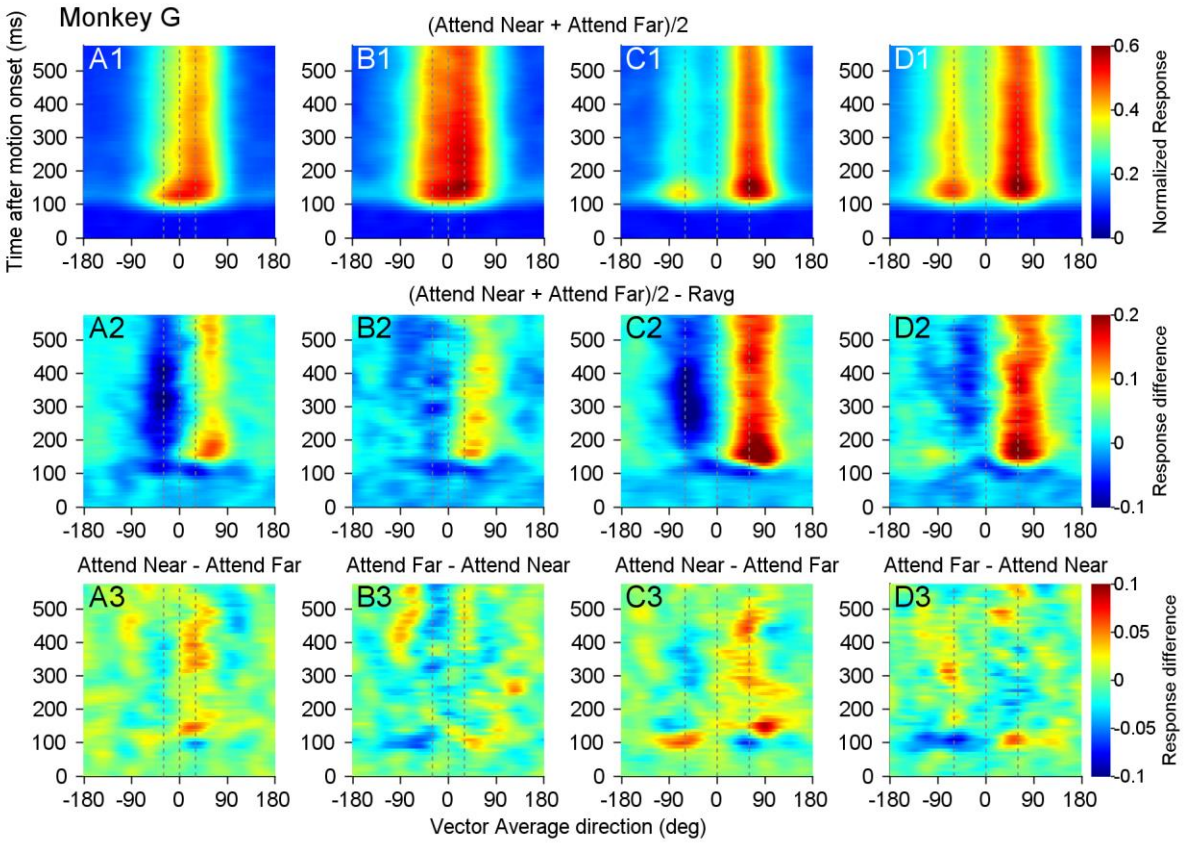

Figure 9. Temporal development of disparity bias and effects of selective attention in monkey G.

A1-D1. Responses to bidirectional stimuli in "Attend Near" (Fig 7 A2 to D2) and "Attend Far" (Fig 7 A3 to D3) conditions averaged together: $(R_{AttendNear} + R_{AttendFar})/2$. **A2-D2.** Difference between the responses from (Fig 9 A1 to D1) and (Fig 8 A4 to D4): $(R_{AttendNear} + R_{AttendFar})/2 - R_{avg}$. **A3, C3.** Difference between the responses from (Fig 8 A2, C2) and (Fig 8 A3, C3): $R_{AttendNear} - R_{AttendFar}$. **B3, D3.** Difference between the responses from (Fig 8 B3, D3) and (Fig 8 B2, D2): $R_{AttendFar} - R_{AttendNear}$. **A1-A3.** Averaged across near neurons under DS60 condition. **B1-B3.** Far neurons DS60. **C1-C3.** Near neurons DS120. **D1-D3.** Far neurons DS120. Vertical dashed lines in each panel indicate the responses to bidirectional stimuli with preferred direction at the near surface/less preferred direction at the far surface ("Near PD"), VA direction (x-axis) 0°, and preferred direction at the far surface/less preferred direction at the near surface ("Far PD"), from right to left, respectively.

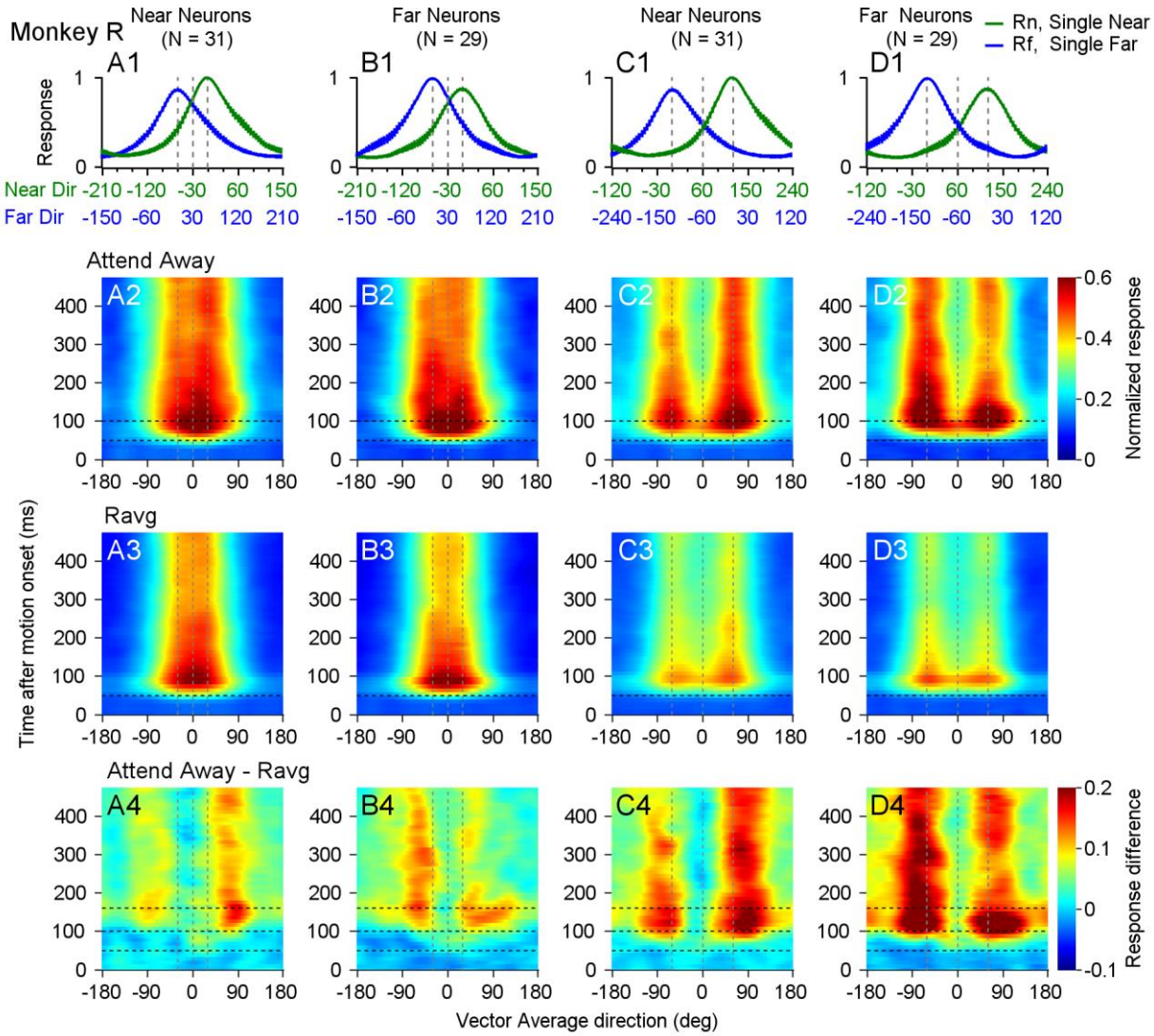

Figure 10. Time course of the response tuning to bi-directional stimuli moving at different depths in monkey R.

A1-D1. Responses to single component near and far directions. Motion directions and population averaged responses are plotted on x and y axes, respectively. **A2-D2.** Responses to bidirectional stimuli from "Attend Away" paradigm. Vector average (VA) direction of two motion directions, time after motion onset, and population averaged responses are plotted on x, y, and z axes, respectively. The bottom and top horizontal dashed lines mark 50 ms (response onset) and 100 ms (near bias onset), respectively. **A3-D3.** Responses to single component near and far directions in (A1-D1) averaged together (R_{avg}). The horizontal dashed lines mark 50 ms (response onset). **A4-D4.** Difference between the responses from (A1 to D2) and (A3 to D3): $R_{AttendAway} - R_{avg.}$ The bottom horizontal dashed lines mark 50 ms (response onset) and the middle and top lines mark 100 ms and 160 ms (window in which the near bias of the near neurons was stronger than the far bias of the far neurons), respectively. **A1-A4.** Averaged across near neurons for DS60 stimuli. **B1-B4.** Averaged across far neurons for DS60 stimuli. **C1-C4.** Averaged across near neurons for DS120 stimuli. **D1-D4.** Averaged across far neurons for DS120 stimuli. Vertical dashed lines in each panel indicate the responses to bidirectional stimuli with preferred direction at the near surface/less preferred direction at the far surface ("Near PD"), VA direction (x-axis) 0°, and preferred direction at the far surface/less preferred direction at the near surface ("Far PD") from right to left, respectively.

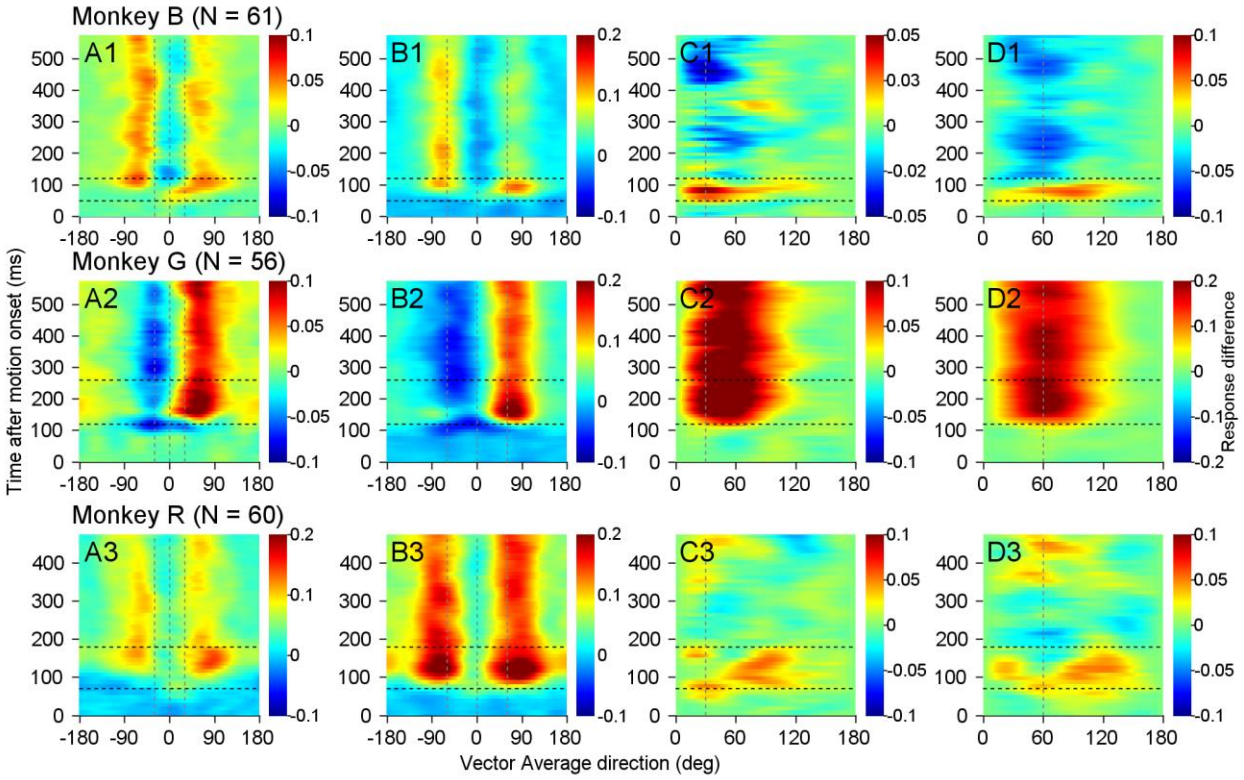

Figure 11. Temporal development of disparity bias across all neurons in three monkeys.

A1, A2. $(R_{AttendNear} + R_{AttendFar})/2 - R_{avg}$ averaged across near and far neurons for DS60 stimuli. **B1, B2**. $(R_{AttendNear} + R_{AttendFar})/2 - R_{avg}$ averaged across near and far neurons for DS120 stimuli. **A3.** $R_{AttendAway} - R_{avg}$ averaged across near and far neurons for DS60 stimuli. **B3.** $R_{AttendAway} - R_{avg}$ averaged across near and far neurons for DS120 stimuli. Vertical dashed lines in A1 to A3, B1 to B3 indicate the responses to bidirectional stimuli with preferred direction at the near surface/less preferred direction at the far surface ("Near PD"), VA direction (x-axis) 0°, and preferred direction at the far surface/less preferred direction at the near surface ("Far PD") from right to left, respectively. **C1-C3.** Difference between the responses from VA= 0° to 180° and those from VA= 0° to -180° in **A1-A3**, respectively. **D1-D3.** Difference between the responses from VA= 0° to 180° and those from VA= 0° to -180° in **B1-B3**, respectively. Vertical dashed lines in C1-C3 indicate VA= 30° and D1-D3 indicate VA= 60°. The horizontal dashed lines indicate the early near bias in all panels.

Attention modulation of neuronal response is object-based.

Figure 4 describes the effect of attention on the full response tuning curve to bi-directional stimuli, as measured by the impact on the weights for the near and far components. We asked, when an animal was cued to attend a stereoscopic depth (binocular disparity) of a surface, whether attention was disparity-based or object/surface-based. If attention was disparity-based (i.e., feature-based attention), we expected to find that when attention was directed to the preferred disparity of a neuron, the neuronal response would be enhanced regardless of the motion direction of the surface. On the other hand, if attention was object/surface-based, we expected to find that

when attention was directed to a stimulus component (i.e., a surface) that elicited a stronger response than the other component, the neuronal response would be enhanced regardless of whether the attended surface was located at the preferred or less preferred disparity of the neuron.

To answer this question, we measured the effect of attention when it was directed to a stimulus component that was located at either the preferred or less-preferred disparity and moving either in the preferred or less-preferred direction of the neuron. We quantified the effect using two attention modulation indices (AMI). One index *AMI_disparity* would be positive across conditions if the effect of attention was disparity-based. Whereas the other index *AMI_surface* would be positive if the effect of attention was surface-based.

$$AMI_disparity = \frac{R_{att_prefdsp} - R_{att_less_prefdsp}}{R_{att_prefdsp} + R_{att_less_prefdsp}} \quad (4)$$

in which $R_{att_prefdsp}$ was the response to the overlapping stimuli when attention was cued to the preferred disparity of the neuron, whereas $R_{att_less_prefdsp}$ was the response when attention was cued to the less-preferred direction.

$$AMI_surface = \frac{R_{att_strongerSurface} - R_{att_weakerSurface}}{R_{att_strongerSurface} + R_{att_weakerSurface}} \quad (5)$$

in which $R_{att_strongerSurface}$ was the response to the overlapping stimuli when attention was cued to a surface that elicited a stronger response, whereas $R_{att_weakerSurface}$ was the response when attention was cued to a surface that elicited a weaker response.

We found that the results from monkey B supported the idea that the attention effect was object/surface-based. Figures 12A and B showed the response tuning curves of two representative neurons from monkey B, one neuron preferred the near disparity (Fig. 12A) and the other preferred the far disparity (Fig. 12B). When attention was directed to a surface that elicited a stronger component response, regardless of whether the surface was located at the preferred or less-preferred disparity of the neuron, the response was always enhanced relative to attending the other surface (Fig. 12A, 12B). This trend was consistent across neuronal populations as captured by always positive *AMI_surface* values (Fig. 12C).

In contrast, when attention was directed to the surface located at the preferred disparity of the neuron (near in Fig. 12A, and far in 12B) and the surface moved in the less-preferred direction giving rise to a weaker component response, the response to both surfaces was reduced relative to attending the other surface (red curve at "Far PD" in Fig. 12A and black curve at "Near PD" in Fig. 12B). Furthermore, when attention was directed to the surface located at the less-preferred disparity of the neuron (far in Fig. 12A, and near in 12B) and the surface moved in the preferred direction giving rise to a stronger component response, the response was nevertheless enhanced (black curve at "far PD" in Fig. 12A and red curve at "near PD" in Fig. 12B). As the result, *AMI_disparity* averaged across the neuronal populations was not always positive (Fig. 12D), suggesting that the attention effect was not disparity-based.

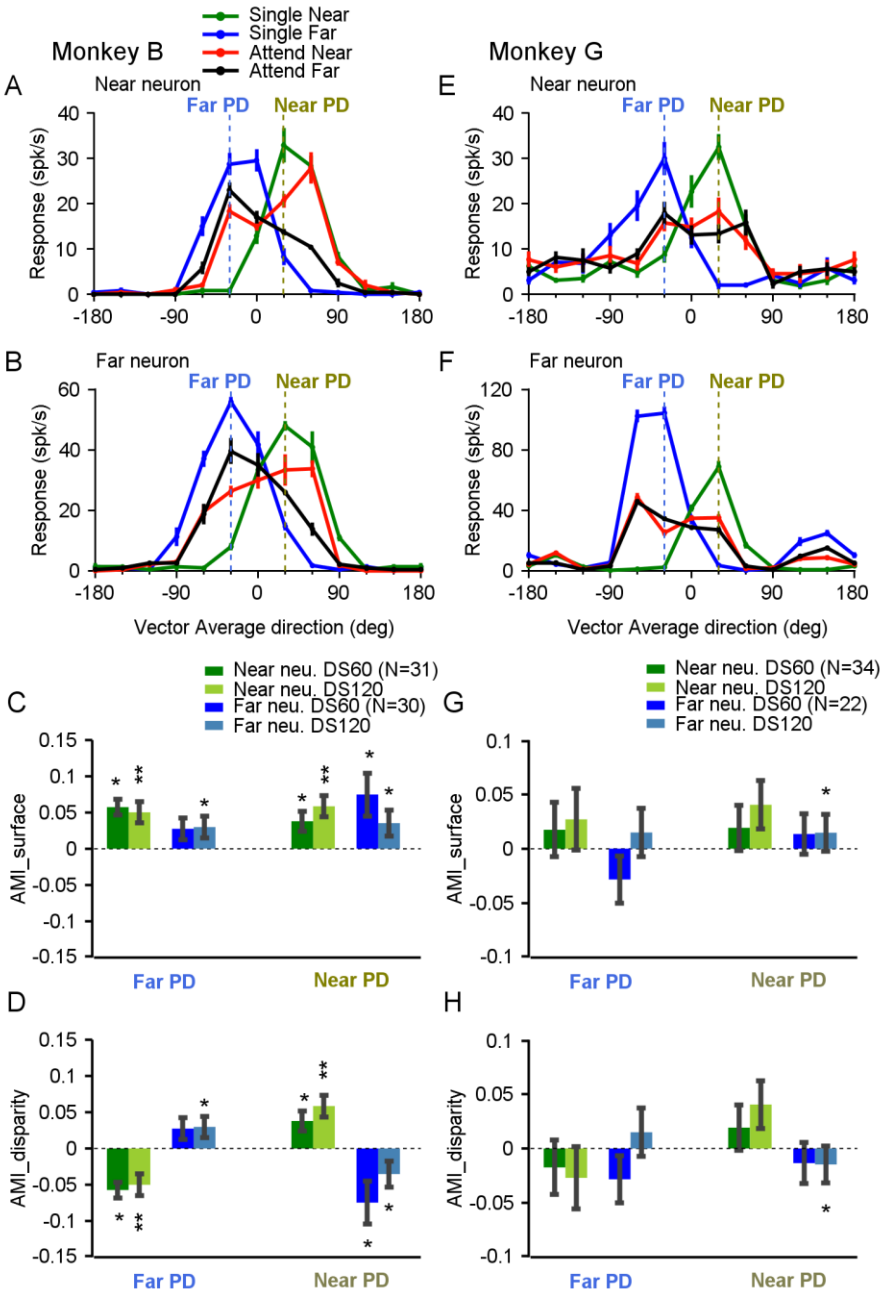

Figure 12. Attention modulation of MT neuronal responses.

A, B, E, F. Tuning curves of four example neurons to bidirectional stimuli separated in depth plotted in a format like that in Fig 2. The vertical dashed lines shown as "Near PD" and "Far PD" indicate responses elicited by the bidirectional stimuli with preferred direction at the near surface/less preferred direction at the far surface and by the stimuli with preferred direction at the far surface/less preferred direction at the near surface, respectively. **C, G.** Surface (object) based attention modulation indices (*AMI_surface* described by Eq. 5) calculated using responses to "Far PD" and "Near PD"- across Near neurons for DS60 and DS120 conditions (shown in two shades of green) and across Far neurons for DS60 and DS120 conditions (shown in two shades of blue). **D, H.** Disparity (feature) based attention modulation indices (*AMI_disparity* described by Eq. 4) calculated using responses to "Far PD" and "Near PD"- across Near

neurons for DS60 and DS120 conditions (shown in two shades of green) and across Far neurons for DS60 and DS120 conditions (shown in two shades of blue). **A-D**. Monkey B. Responses from 0 to 600 ms of motion period were used to calculate AMIs. **E-H**. Monkey G. Responses from 110 to 410 ms of motion period were used to calculate *AMI*s. (**) indicates p<0.01, (*) indicates p<0.05, no asterisk indicates p>0.05, one-sided signed rank test to indicate significance of difference from zero.

The attention effect found in monkey G was weaker than that in monkey B. Nevertheless, the effect of attention in monkey G was clearly visible in most of the conditions during the time window from 110 ms to 410 ms after the motion onset (Fig. 9A3, C3, D3). We therefore used the responses during this time window to calculate the direction tuning curves (Fig. 12E, F) and the AMI. Except for the far neurons at the angular separation of 60º, the trend of AMI of monkey G (Fig. 12G, H) was consistent with monkey B (Fig. 12C, D) and supported the idea that the attention modulation was object/surface-based. Note that, for most of the conditions, the effect found in monkey G did not reach statistical significance.

Fitting the neural responses to two moving surfaces using a unified model

From the results above, an MT neuron's response to overlapping moving stimuli separated in depth can be described by a weighted sum of the neuron's responses to the individual stimulus components presented alone. We found that the weights were dependent on the disparity preference of the neuron to single surface (Fig. 5) and selective attention (Fig. 4 and Fig. 12). While the general trend was consistent across animals, we also noted some pronounced individual differences. Specifically, for monkey G, both near and far neurons showed a dominant effect of near bias, albeit stronger near bias for the near neurons than the far neurons (Fig. 5). Whereas, for monkey B, the near neurons showed a near bias and the far neurons showed a far bias. We sought a unified model that can explain these results.

The divisive normalization model (Carandini and Heeger, 2011) has been used to explain a wide array of phenomena, including neuronal responses elicited by multiple visual stimuli (Britten and Heuer 1999; Heuer and Britten 2002; Busse et al. 2009; Xiao et al. 2014; Xiao and Huang 2015; Bao and Tsao 2018; Wiesner et al. 2020; Huang et al. 2023) and the effects of attention (Reynolds and Heeger 2009; Lee and Maunsell 2009; Ni et al. 2012; Ni and Maunsell 2019). However, in the normalization model, while the division by the activity of a population of neurons in the denominator (i.e., normalization) is well established, what accounts for the numerator is unclear. In the case of describing the response to multiple stimuli, the signal strength such as luminance contrast or motion coherence of each stimulus component was typically used in the numerator (e.g., Busse et al. 2009; Xiao et al. 2014). A caveat is that it is not always clear how to define the signal strength of a sensory stimulus (Wiesner et al. 2020). We have suggested that the weighting to a stimulus component of multiple stimuli is proportional to the activity of a population of neurons, referred to as the "weighting pool" (Xiao et al. 2014; Wiesner et al. 2020; Huang et al. 2023), and divisively normalized by the activity of the "normalization pool" as in the standard normalization model. The nature and scope of the "weighting pool" are not understood. Here, we further developed this idea and used the size of the "weighting pool" as a model parameter to account for the MT responses from monkeys B and G (Eq. 6 and 7).

$$R_{(n_a,f)} = \frac{\beta_{An} \bullet S^m_{near}}{\beta_{An} \bullet S^m_{near} + \alpha \bullet S^m_{far} + \sigma} R(\theta_n) + \frac{S^m_{far}}{\beta_{An} \bullet S^m_{near} + \alpha \bullet S^m_{far} + \sigma} R(\theta_f) + c \qquad (6)$$

$$R_{(n,f_a)} = \frac{S_{near}^m}{S_{near}^m + \alpha \bullet \beta_{Af} \bullet S_{far}^m + \sigma} R(\theta_n) + \frac{\beta_{Af} \bullet S_{far}^m}{S_{near}^m + \alpha \bullet \beta_{Af} \bullet S_{far}^m + \sigma} R(\theta f) + c \quad (7)$$

in which $R_{(n_a,f)}$ and $R_{(n,f_a)}$ are the model predicted responses to the bi-directional stimuli when the near surface and the far surface are attended, respectively. n_a or f_a denotes that either the near or far surface is attended. $R(\theta_n)$ and $R(\theta_f)$ are the measured responses elicited by the near and far components alone, moving in directions θ_n and θ_f, respectively. m, σ, and c are model parameters with the constraints of 0 < m < 100, σ > 0, and c > 0. A positive parameter α scales the relative contributions of S_n and S_f to the denominators as in tuned normalization (Ni et al. 2012; Rust et al. 2006; also see Carandini et al. 1997). β_{An} and β_{Af} are positive attentional weighting parameters when the near and far surfaces are attended, respectively. We derived the values of $\beta_{An}$and β_{Af} from the weights of the LWS model fitting (see Methods Eq. 15a and 15b).

In equations 17 and 18, S_{near} and S_{far} were the summed population neural responses of the "weighting pool" (***pR***) elicited by the stimulus disparity of the near and far components, respectively (Eq. 11, 12). Generally, for a given neuron *k*, S_k was the summed population neural responses of ***pR*** elicited by a single stimulus disparity d_{stim}, and weighted by a Gaussian window centered on the preferred disparity of the neuron *k* (i.e., d_{pref_k}) (Eq. 8-10). The standard deviation v of the Gaussian weighting function ***G*** was a model parameter and determined the broadness of ***G*** (Eq. 9), with the constraint of the disparity borders (from -1.6º to 1.6º) (see Methods). On one extreme when v was very large, the weighting pool included neurons covering a broad range of preferred disparities (orange lines in Fig. 13A for two example d_{pref_k} values), referred to as the "global pooling". On the other extreme when v was close to zero, the weighting pool only included neurons that had the same preferred disparity as the neuron *k*, referred to as the pure "local pooling" (brown lines in Fig. 13A). We determined the optimal v that gave rise to the best fit of the data of each animal and compared the optimal v between monkeys B and G (Fig. 13B, C) (see Methods).

The neuronal response of a population of neurons to a single stimulus disparity d_{stim} was a vector of length *N* and denoted as:

$$\boldsymbol{pR}(d_{\boldsymbol{stim}}) = [f_i(d_{stim},\ d_{pref,\ i})],\quad i = 1 \text{ to N}. \quad (8)$$

f_i was the disparity tuning curve of neuron *i*, in response to single disparities. $d_{pref,\ i}$ was the preferred disparity of neuron *i*. Because the number of neurons in our data set is relatively small, the percentage of the near and far neurons in our data may not reflect the true distribution of the disparity preference of MT neurons. We therefore used data of the disparity tuning curves of a large sample of MT neurons (*N* = 479) from DeAngelis and Uka (2003) to estimate ***pR***.

The Gaussian weighting function centered on the disparity d_{pref} of a neuron was a vector of length *N* and defined as:

$$\boldsymbol{G}(d_{pref}) = [\frac{1}{\sqrt{2\pi v}} e^{\frac{-(d-d_{pref})^2}{2v^2}}],\ d = -1.60\ to\ 1.60 \text{ and matched } dpref, i\ in\ \boldsymbol{pR} \quad (9)$$

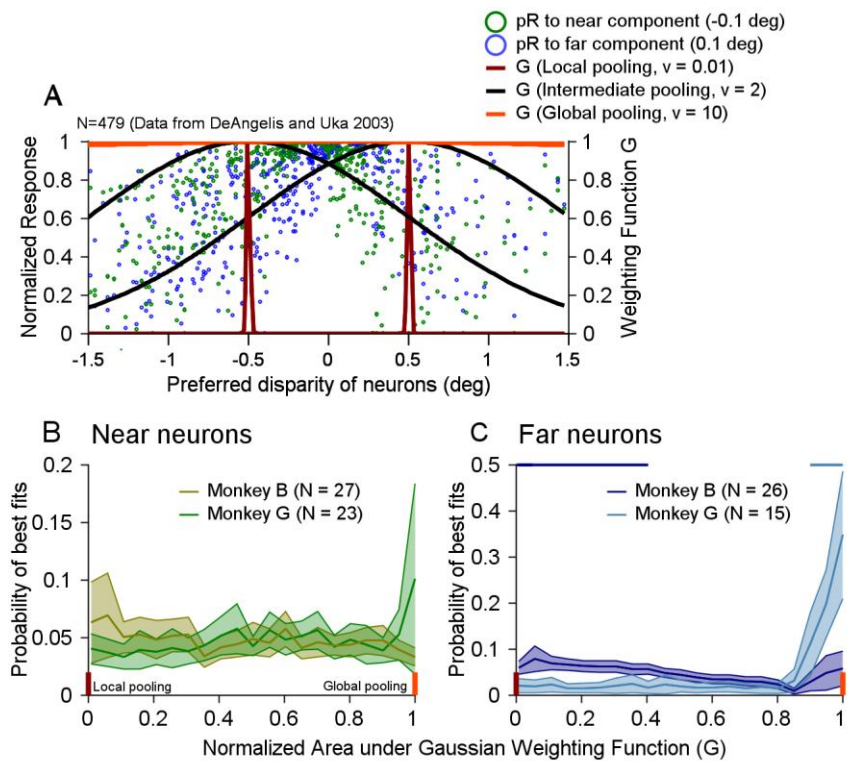

Figure 13. Probability distribution of sizes of the weighting pools from the divisive normalization model.

A. Green and blue dots show the normalized responses of 479 MT neurons (DeAngelis and Uka 2003) to -0.1° and +0.1° disparities moving in their preferred directions, denoted as pR (Eq. 8). Orange, brown, and black lines show examples of Gaussian weighting function (***G***) of global, local, and intermediate pooling strategies (Eq. 9). The area under ***G*** represents the size of the weighting pools. **B**. Probability distributions of the area under ***G*** s resulting from divisive normalization model (DNM) fits of the bidirectional tuning curves of individual neurons (see Methods). Yellowish green and green lines indicate the probability distributions from the fits of monkey B and G's near neurons, respectively. The error bands are 95% confidence intervals. **C**. Far neurons. Dark and light blue curves are for monkey B and G. The flat lines on top indicate the portions of significant difference between the monkeys. The colors of the flat lines match that of the monkey with significantly higher probability values (p<0.05, 95% confidence intervals estimated by bootstrapping).

For a given neuron k, S_k was the dot product of $G(d_{pref_k})$ and $pR(d_{stim})$, where d_{pref_k} is the preferred disparity of neuron k.

$$S_k(d_{stim}, d_{pref_k}) = \boldsymbol{G}(d_{pref_k}) \bullet \boldsymbol{pR}(d_{stim}) \qquad (10)$$

In our study, $d_{stim} = \pm 0.1^0$, so

$$S_{near}(d_{pref_k}) = S_k(-0.1^0, d_{pref_k}) \qquad (11)$$

$$S_{far}(d_{pref_k}) = S_k(0.1^0, d_{pref_k}) \qquad (12)$$

Due to the constraint of the range of preferred disparities in the data set, the area under the Gaussian weighting window ***G*** truncated by the disparity borders was a better descriptor of the size of the weighting window than the standard deviation ν (see Supplementary Fig. 2 for the relationship

between the two). We, therefore, varied the area under $\boldsymbol{G}$ to find the best fit of the neuronal response.

The model fitted the neuronal responses to two surfaces from monkeys B and G reasonably well. The mean PV was 89 % (STD = 11.2) for monkey B and 80% (STD = 17.5) for monkey G. We compared optimal weighting pool size that gave rise to the best fit across the near neurons (Fig. 13B) and the far neurons (Fig. 13C) for monkeys B and G. For the near neurons, monkey B had more neurons that were best fitted with local pooling and monkey G had more neurons that were best fitted with global pooling, but the differences did not reach the significance level ($p > 0.05$; 95% confidence intervals estimated by bootstrapping) (Fig. 13B). For the far neurons, local pooling fitted best for significantly more neurons from monkey B than monkey G (at normalized area of weighting window less than 0.4, $p < 0.05$), and global pooling fitted best for significantly more neurons for monkey G than monkey B (at weighting window area greater than 0.9, $p < 0.05$) (Fig. 13C). Remarkably, for 11 of 15 far neurons (70%) from monkey G, the optimal area of the weighting window was greater than 0.85, suggesting that global pooling was best to account for the results of far neurons from monkey G. In contrast, local and intermediate pooling was best to account for the results from monkey B. Taking together, we showed that a unified model with a variable size of the weighting pool and divisive normalization can explain our results of the disparity bias and the individual difference between the animals.

Discussion

Disparity bias and implication on the general rules of representing multiple visual stimuli

Our laboratory has previously found that when two overlapping random-dot stimuli move in different directions at the same depth, MT neurons show a robust response bias toward the stimulus component that has higher motion coherence or luminance contrast (Xiao et al., 2014). Because nearly all MT neurons respond more strongly to higher motion coherence (Britten et al., 1992, 1993; Xiao et al., 2014) and contrast (Cheng et al., 1994; Heuer and Britten, 2002; Sclar et al., 1990), the stimulus preference is consistent at the levels of individual neurons and neuronal populations. However, for many other stimulus features such as binocular disparity, different neurons prefer different values. Our current study helps to establish the encoding rule of representing multiple stimuli when different neurons have different preferences for a stimulus feature.

We made a novel finding that MT neurons showed a disparity bias toward one of two overlapping surfaces at different depths and the bias was positively correlated with neuron's preference for the disparity of a single surface when presented alone (Fig. 5). Although we found significant individual differences among animals, this positive correlation was common in all three animals. In two animals (B and R), the near neurons showed a near bias, and the far neurons showed a far bias. In the third animal (G), almost all neurons showed a near bias, but the near neurons showed a stronger near bias than the far neurons. The positive correlation between the bias in response to two stimuli and the neuron's preference for a single stimulus may be a general property applied to features other than binocular disparity. For example, in another study, our laboratory placed two spatially separated stimuli moving in different directions in the RFs of MT neurons. The neuronal responses to two stimuli moving in a 2D plane showed a robust spatial bias,

which was positively correlated with the neurons' spatial preferences for the individual stimuli (Wiesner and Huang, 2019, SFN abstract). Since depth is another spatial dimension in the 3D space, the disparity bias found in the current study may also be considered a "spatial bias". The spatial bias could provide a useful means to segment multiple visual stimuli placed at different locations in 3D space.

An extended normalization model and the neural mechanism underlying the disparity bias

In the standard divisive normalization model, the response to multiple stimuli is described by a weighted sum of the responses elicited by the individual stimulus components. The weight is proportional to the signal strength (such as contrast) of each stimulus component, normalized by a combination of the signal strengths of multiple stimuli (Busse et al., 2009; Carandini and Heeger, 2011; Ni et al., 2012; Xiao et al., 2014; Bao and Tsao, 2018). In terms of the neural implementation of the divisive normalization model, it has been proposed that the summed response of a population of neurons, referred to as the normalization pool, serves as the denominator in the divisive normalization equation (Heeger, 1992; Carandini et al., 1997; Simoncelli and Heeger, 1998; Rust et al., 2006; Kouh and Poggio, 2008; Bao and Tsao, 2018; Wiesner et al., 2020). However, the neural implementation of the numerator in the normalization equation has been unclear when multiple visual stimuli are involved. We and other investigators have suggested that the summed response of a population of neurons elicited by a stimulus component may serve as the numerator and determine (together with the normalization) the weight of that component (Xiao and Huang, 2014; Bao and Tsao, 2018; Wiesner et al., 2020). However, little is known about the nature of the neuronal population that contributes to the numerator. A common and usually implicit assumption is that the neuronal population in the numerator is the same as that in the denominator (i.e. the normalization pool). In the current study, we extended the standard normalization model and made a novel proposition that the pool size of the neuron population in the numerator (i.e. the weighting pool) can be variable and is not necessarily the same as the normalization pool. With this assumption, the weighting for a stimulus component may depend on a group of neurons that have similar feature selectivity as the neuron under study (i.e. local pooling), or a group of neurons that have feature selectivity covering a full range of possible values (i.e. global pooling), or somewhere in between. With local pooling, the response of a neuron to two stimuli would show a bias toward the more preferred feature value of the neuron in response to the single stimulus (as found in monkeys B and R). With global pooling, the response bias to two stimuli would be determined by the preference of a population of neurons that have a full representation of the stimulus feature. In the case of binocular disparity, MT neurons tend to have more neurons that prefer the near disparity (DeAngelis and Uka, 2003). The summed response of the full population tends to be stronger to the near disparity than the far disparity and is invariant to the disparity preference of the individual neurons under study. As a result, global pooling makes neurons tend to show near bias regardless of their disparity preferences for a single stimulus. When the pool size is broad enough to reflect the overall near preference of a large population of neurons, but not completely invariant to the disparity preference of the neuron under study, the neuronal response to two stimuli would show a near bias and a positive correlation with individual neuron's disparity preference for a single stimulus (as found in monkey G). Our model provides a unified explanation of the disparity bias across animals. In the future, it would be interesting to understand what factors (such as experience, cognition, and other individual differences) determine the size of the weighting pool. It is also conceivable that the pooling size may be different for different stimulus features. E.g. we recently

showed evidence that the neural representation of multiple speeds of overlapping stimuli in MT is consistent with a scheme of global pooling (Huang et al., 2023).

Modulation of MT response by object-based (surface-based) attention

Attention not only can select a spatial location or a stimulus feature, but it also can select a visual object (Duncan, 1984; Cavanagh et al., 2023). Behavioral effects of object-based attention have been demonstrated using transparent motion stimuli (Valdes-Sosa et al., 1998, 2000; Mitchell et al., 2003, 2004). Using similar stimuli, Wannig et al. (2007) showed that the responses of MT neurons can be modulated by object-based attention directed to a moving surface of two overlapping stimuli. Modulation of neuronal responses by object-based attention has also been found in V1 (Roelfsema et al., 1998) and V4 (Fallah et al., 2007). Our study showed new evidence of response modulation by object-based attention in MT. Importantly, our visual stimuli and experimental paradigm allowed us to distinguish the effect of object-based attention from feature-based attention.

Responses of MT neurons can be modulated by feature-based attention to motion direction (Treue and Martinez-Trujillo, 1999; Martinez-Trujillo and Treue, 2004), and binocular disparity (Ruff and Born, 2015). At the neuron population level, attending to the preferred direction of an MT neuron enhances the response to visual stimuli in the RF relative to attending to the null direction, regardless of whether the RF stimulus moves in the preferred or null direction of the neuron (Martinez-Trujillo and Treue, 2004). The same result was found for attending to binocular disparity (Ruff and Born, 2015). These results are consistent with the "feature-similarity gain (FSG) model" of attention (Martinez-Trujillo and Treue, 2004; Maunsell and Treue, 2006). In our study, however, we found that attending to the more preferred disparity of MT neurons did not always enhance MT responses to two moving surfaces. When the surface at a more preferred disparity moved in a less preferred direction, attending to the more preferred disparity reduced MT response. Conversely, when the surface at a less preferred disparity moved in the preferred direction, attending to the less preferred disparity enhances MT response (Fig X). Therefore, the attention modulation was not due to feature-based attention to binocular disparity. To account for the neural response modulation, the attention initially directed to a given binocular disparity of a stationary surface must spread to the motion direction of the attended surface of the overlapping stimuli, although the motion direction was never explicitly cued. Because the motion direction and the cued binocular disparity belong to the same surface, selecting the surface by attention would allow attention to spread to other features of the same object. Whether attention enhanced or reduced the neural response to two surfaces was dependent on whether the attended surface elicited a stronger or weaker component response than the other surface, rather than whether the attended surface was at the preferred or less preferred disparity of the neuron.

Since stereoscopic depth can be considered a spatial dimension in 3D space, may the effect of attention modulation found in our study be due to spatial attention? In response to two 2D stimuli placed at different locations within the RF, the neuronal response in MT (Treue and Maunsell, 1996; Seidemann and Newsome, 1999) and V2 and V4 (Moran and Desimone, 1985; Luck et al., 1997; Reynolds et al., 1999) is enhanced (or reduced) when attention is directed to the spatial location where a stimulus component is a preferred (or null) stimulus of the neuron when presented alone. It has been shown that these results can be explained by the biased competition model (Desimone and Duncan, 1995; Reynolds et al., 1999) and the model of divisive

normalization (Ghose and Maunsell, 2008; Lee and Maunsell, 2009; Reynolds and Heeger, 2009; Ni et al., 2012). Our finding that attending to a surface eliciting a stronger (or weaker) component response when presented alone enhanced (or reduced) the response to overlapping 3D stimuli is consistent with these previous studies. Our study made two new advancements. First, it extended the finding to 3D stimuli with attention directed to the feature of binocular disparity. Second, previous studies using 2D stimuli did not measure the spatial preferences of the neurons. In contrast, our study directed animals' attention to the more preferred or less preferred disparity of the neurons and showed that the attention modulation was not dependent on the attended disparity, but dependent on the combined stimulus features of the attended surface as a whole. Regarding whether the attention modulation found in our study was due to spatial attention or object-based attention, we think the distinction may be more semantic than mechanistic. One can think of a surface in our study either as an object or a spatial location in depth. In the previous studies, although attention was directed to a spatial location within the RF, it was also possible that attention selected the visual stimulus as an object at the attended location which allowed spatial attention to spread to other features of the stimulus such as motion direction or orientation. Cavanagh and colleagues (2023) have recently suggested that spatial attention may rely on object-based attention.

Functional implication of disparity bias on segmentation and figure-ground segregation

It becomes easier to segment two overlapping surfaces when they are moving at different depths than at the same depth (Hibbard and Bradshaw, 1999; Greenwood and Edwards, 2006). The neural representation of two surfaces moving transparently in different directions and at different depths is distributed in the responses of populations of neurons that are selective for motion directions and binocular disparities. Without disparity cues, the visual system can only rely on motion cues to segment the overlapping surfaces (Xiao and Huang, 2015). When two moving surfaces are located at different depths, even without the disparity bias, MT neurons that prefer the binocular disparity of one surface carry more information about the motion direction of that surface and therefore aid in segmentation. However, the benefit can be limited when the disparity difference between two surfaces and the angular separation between two motion directions are small. The disparity bias that we found (from monkeys B and R) further enhances the neural representation of the motion direction at the surface located at the more preferred disparity of the neurons. This disparity bias, which is independent of attention modulation, could help further partition the neural representation of multiple stimuli into distributed responses across different neuronal populations and therefore facilitate segmentation. Together, these mechanisms may provide a neural basis for the perceptual benefit of depth cues on segmentation.

Three lines of evidence suggest that the near surface of overlapping stimuli may be better represented than the far surface. First, in monkey G, we found a predominant near bias across near and far neurons. The overall near bias could facilitate the segmentation of the near surface, which is consistent with the better performance of monkey G in discriminating the motion direction of the near surface than the far surface of overlapping stimuli. Second, for animals like monkeys B and R, near surface may be better represented than the far surface because more neurons tend to prefer near disparity over far disparity across visual areas of V1, V2, V4 (Prince et al., 2002; Chen et al. 2008; Gonzalez et al., 2010; Samonds et al., 2012; Hinkle et al., 2005; Tanabe et al., 2005), and MT and MST (Maunsell and Van Essen, 1983b; DeAngelis and Uka, 2003; Gonzalez et al., 2001). Since near neurons tend to show near bias and far neurons tend to show far bias, having

more near neurons in the population would better represent the near surface of overlapping stimuli. Third, when combining all neurons in our dataset for each of the three animals, we found an initial near bias relative to the average of two component responses (Fig. 11). This finding suggests that, at least in the early response, the near surface is better represented than the far surface, making it likely easier for the near surface to be segregated from the far surface, or to be selected by attention. Figural objects in natural scenes are more likely to reside at near disparity than far disparity relative to the ground region (Huang et al., 2019 SFN abstract). A better neural representation of the near surface in the visual cortex may reflect a strategy that the visual system uses to exploit the statistical regularity of natural vision and to better serve the function of figure-ground segregation.

Methods

Three male adult rhesus monkeys (Macaca mulatta) were the subjects in the neurophysiological experiments. We followed experimental protocols approved by the Institutional Animal Care and Use Committee of the University of Wisconsin–Madison and conformed to U.S. Department of Agriculture regulations and the National Institutes of Health guidelines for the care and use of laboratory animals. Procedures for surgical preparation and electrophysiological recordings were akin to those described previously (Xiao et al. 2015). We implanted a head post and a recording cylinder during sterile surgery with the animal under isoflurane anesthesia. For electrophysiological recordings from neurons in area MT, we took a vertical approach and used tungsten electrodes (1–3 M; FHC). We identified area MT by its characteristically large portion of direction-selective neurons, small RFs relative to those of neighboring medial superior temporal cortex (area MST), its location at the posterior bank of the superior temporal sulcus, and visual topography of the RFs (Gattass & Gross, 1981). We amplified electrical signals and identified single units with a real-time template-matching system and an offline spike sorter (Plexon). We monitored the animal's eye position using a video-based eye tracker (EyeLink, SR Research) at a rate of 1000 Hz. For some of the recording sessions from monkey B, we tracked both the left and right eye positions which were then used to calculate the horizontal vergence values (left eye X position-right eye X position).

Experimental procedures

We used a real-time data acquisition program, "Maestro" to control stimulus presentation and data acquisition. For all experiments, we presented visual stimuli on a 25-inch CRT monitor at a viewing distance of 63 cm. The monitor resolution was 1024 x 768 pixels, with a refresh rate of 100 Hz. We generated the visual stimuli on a Linux workstation using the OpenGL application that communicated with an experimental control computer. We did the luminance calibration of the CRT monitor with a photometer (LS-110, Minolta) and then used a standard display gamma value of 2.2 for gamma correction.

After we isolated the spike waveforms of a single neuron, we first characterized the neuron's direction selectivity by interleaving trials of a 30° x 27° random-dot patch (RDP), covering the entire monitor, moving in different directions at a step of 45° and a speed of 10°/s. The direction selectivity and preferred direction (PD) were determined using MATLAB (MathWorks). We then characterized the speed tuning of the neuron using a random dot patch moving at different speeds (1, 2, 4, 8, 16, 32, or 64°/s) in the PD of the neuron. Using a cubic spline, we took the preferred speed (PS) of the neuron as the speed that evoked the highest firing

rate in the fitted speed-tuning curve. Next, we mapped the receptive field (RF) location of the neuron by recording responses to a series of 5° × 5° patches of random dots that moved in the PD and at the PS of the neuron whose location we varied randomly to tile the screen (35×25°) in 5° steps without overlap. We then interpolated the raw map of these responses at an interval of 0.5° to obtain the location with the highest firing rate response as the center of the RF.

We used green and red anaglyph filters (Kodak Wratten filters, nos. 25 and 58) to create stereoscopic depth on the monitor using horizontal disparity. To achieve a disparity of + n° or - n°, we used two identical dot patterns, one in green and the other in red with the center of the red dot pattern offset horizontally by +n° or -n° relative to that of the green dot pattern, respectively. As the animals viewed the stimuli through a green filter on the left eye and a red filter on the right eye, only one set of dots was visible to each eye creating a binocular disparity that resulted in depth perception. Crosstalk between the two eyes, as viewed through the filters, was 14.5%, 9.6%, and 9.6% for monkeys G, B, and R, respectively. We determined the selectivity of an MT neuron to binocular disparity by measuring its responses to a series of RDPs moving in its preferred direction and at its preferred speed (often within 5 to 20°/s) at fifteen different disparities from -1.5° to +1.5°.

Visual stimuli

Transparent motion stimuli constituted two overlapping circular random dot patches (RDPs) of size 15° moving at two different depths: one at -0.1° binocular disparity (near) and the other at 0.1° binocular disparity (far) relative to the fixation point on the monitor (Fig 2 A to D). We refer to the constituent RDPs as 'stimulus components': the one at near disparity as 'near component' and the one at far disparity as 'far component'. Each RDP's dot density was 0.89 dots/deg^2 with infinite dot lifetime and had 100% coherence. The visual stimuli were usually centered on the fixation spot and sometimes shifted toward the RFs for 1 to 2°. As a result, the visual stimuli covered the RFs but usually were not centered on the RFs. The speed of the motion stimuli was 10°/s in most sessions and 12°/s in a few sessions.

Behavioral tasks

In the discrimination task with attention cue (Fig 1 A and B), we trained Monkey B and G to report the motion direction of the RDP (stimulus component) at cued disparity (+ 0.1° or - 0.1°). Each trial started with a fixation dot in the center of the screen and stationary reference dots (not shown in the figure). The animal had to maintain fixation within 1°x 1° window around the dot to continue the trial. As a cue for attention, a static circular RDP with a diameter of 15° appeared for 500 ms at either near plane (-0.1° disparity) or far plane (0.1° disparity) referred to as "Cue Near/Attend Near" and "Cue Far/Attend Far" conditions, respectively. To aid depth perception, stationary reference dots at zero disparity covered the rest of the monitor. This was followed by 300 ms of blank screen with a fixation dot. Then, a single component RDP at the cued disparity (+0.1°: Single Near or -0.1°: Single Far) or two overlapping RDPs at +0.1° and -0.1° disparities appeared stationary for 500ms. And they started moving for 600ms in one of the 12 directions: 0 to 360° at 30° step. After the motion period, the stimuli were off, and 12 reporting targets arranged from 0 to 360° at 30° step along a circle of 10° diameter, appeared for 450 ms for monkey B and 600 ms for monkey G. During this time window, the animals had to report the motion direction of the cued component (Near or Far) by making a saccade to the corresponding target and holding fixation within 1.5°x 1.5° target window for 350ms to receive a juice reward. We used two angle separations between the overlapping motion directions (60°/DS60 or 120°/DS120) to reduce the

chances of the animals predicting the direction of the component at cued disparity just by attending to the other/un-cued component. For each angle separation, we used two configurations to control the effects of clockwise (c) or counter-clockwise arrangement of overlapping stimuli on MT neuronal responses (Xiao et al 2015): 1. Near component moving clockwise and far component moving counter-clockwise (Near C-Far CC), and 2. Near component moving counter-clockwise and far component moving clockwise (Near CC-Far C).

In the attention-away task, the stimuli were centered on MT neurons RFs. To direct the animal's attention away from the RF, we trained Monkey R to perform a two-alternative forced choice (2-AFC) task of discriminating whether the motion direction of an RDP, presented in the opposite visual hemifield, was clockwise (C) or counter-clockwise (CC) to vertically upward direction. Every trial began with the appearance of a fixation dot at the center of the screen and the reference stationary dots at zero disparity. The animal fixated within 1°x 1° window of the dot for 200 ms. Then the stimuli in the RFs ("Single" or "Overlapping" disparity motion stimuli) appeared along with an "attention stimulus": a random-dot patch with a diameter of 5°, placed at 10° eccentricity in the opposite hemifield. Both stimuli remained stationary for 250 ms and then the "attention stimulus" moved either clockwise or counterclockwise from upward direction for 500 ms by 10°, 15°, or 20° offset in randomly interleaved trials. Then, all the stimuli were turned off, and two reporting targets appeared on the left and right side of the FP. The animal made a saccade to the left (or the right) side to indicate if the motion of the "attention stimulus" was counterclockwise (or clockwise) of upward direction and maintained fixation on the correct target for 200ms to receive a juice reward.

Experimental design and statistical analysis

Neuronal response (firing rate) was calculated during the stimulus motion period (600 ms for the discrimination task with attention and 500 ms for attention away task) averaged across repeated trials. We constructed the response tuning curves to unidirectional stimuli (Single component) and to bidirectional stimuli (Overlapping) and fitted the raw direction tuning curves using cubic splines at a resolution of 1°. For each vector averaged (VA) direction of the overlapping motion directions, we determined the responses elicited by the bidirectional stimuli and the constituent unidirectional stimulus components. To average the direction tuning curves across neurons, we rotated the spline-fitted tuning curve elicited by the bidirectional stimuli such that the VA direction of 0° was aligned with the PD of each neuron. We then normalized neuronal responses by each neuron's maximum response to near and far components and averaged the aligned, normalized tuning curves across neurons. We pooled the responses of Near C-Far CC and Near CC-Far C conditions for population averaged tuning curves in Fig 3. The resulting tuning curves always had the near component at C side and the far component at CC side for visualization. To do so, we first horizontally flipped the tuning curves to the bidirectional and unidirectional stimuli of neurons of Near CC-Far C conditions, along the axis of VA direction. We then averaged the flipped tuning curves together with the tuning curves of Near C-Far CC condition.

To examine the time-course of the response tuning to the bidirectional stimuli, we calculated the response tuning for each individual neuron using the trial-averaged firing rates within a 50ms time window, sliding at a step of 10-ms, and normalized the responses by the maximum firing rate of the near and far components response across all time windows. We then pooled the responses of Near C-Far CC and Near CC-Far C conditions in the same way as we did for the populations averaged tuning curves mentioned above.

LWS model

To quantify the relationship between the responses elicited by the bidirectional stimuli and those elicited by the individual stimulus components, we fitted the direction tuning curves using a linear weighted summation (LWS) model (Xiao et al. 2014) by minimizing the sum of squared error:

$$R_{nfpred}(\theta_n, \theta_f) = w_n R_n(\theta_n) + w_f R_f(\theta_f) + c \qquad (13)$$

R_{nfpred} is the response to the bidirectional stimuli predicted by the model; R_n and R_f are the measured responses elicited by the near and far components, respectively, when presented alone; θ_n and θ_f are the motion directions of the near and far components; w_n and w_f are the response weights of the near and far components, respectively; and c is a positive number. b in the SNL model is the "nonlinear interaction coefficient" that determines the sign and strength of the multiplicative interaction between the component responses.

Divisive normalization model (DNM)

We fitted each neuron's response tuning curves to the bidirectional stimuli using a modified divisive normalization model (see Results). Equations 17 and 18 were used to fit each of the four bidirectional tuning curves of a neuron (described in Fig 2: DS60 Near C-Far CC, DS60 Near CC-Far C, DS120 Near C-Far CC, and DS120 Near CC-Far C) under "Attend Near" and "Attend Far" conditions, respectively. Hence, each neuron contributed to the fits of eight bidirectional tuning curves presented in the results.

When fitting the DNM model (Eq. 17 and 18) to each neuron's bi-directional response tuning, we divided the search space for parameter v (with bounds from v =0.01 to 40) to result in equal steps (s) of the area covered by the gaussian weighting function $\boldsymbol{G}$ (See Eq. 20). This is because the area covered by the gaussian weighting function $\boldsymbol{G}$ better represents the size of the weighting pool than the standard deviation (v) (see Supplementary Fig 2). For each v value in the search space (v =0.01 to 40 at a step of s), we used the constrained minimization tool "fmincon" (MATLAB) to minimize sum of squared error (SSE) of Eq 17 or 18, varying all other free parameters of the model. To identify the v values resulting in the least SSE, we plotted the resulting SSE as a function of the values of v in the search space, referred to as SSE(v). Based on SSE(v), we calculated a probability distribution of the v values (pdf(v)) using the steps below, accounting for multiple v values resulting in similar fits (i.e., SSE values). First, we normalized the SSE(v) function between 0 and 1 to get $\mathrm{SSE}_{\mathrm{norm}}(v)$. Using a threshold of 0.05, for v values with $\mathrm{SSE}_{\mathrm{norm}}(v)$<=0.05, we set $f(v)$=1 and for all other v values, $f(v)$=0. We then normalized $f(v)$with sum of $f(v)$ across all v values to get the probability of best fit at each v value i.e., $\mathrm{pdf}(v) = \frac{f(v)}{\Sigma f(v)}$. The pdf($v$) functions obtained for each tuning curve of each neuron are averaged across near and far neurons to get $\mathrm{pdf}_{\mathrm{near}}(v)$ and $\mathrm{pdf}_{\mathrm{far}}(v)$ for each monkey plotted against area under $\boldsymbol{G}$ (Fig 13B and 13C). To evaluate the statistical significance of the difference of pdfs between the monkeys, we used bootstrapping where we randomly sampled the pdf values (of a neuronal set) 1000 times with replacement and calculated the 95% confidence intervals for each v value.

<u>Attentional weighting parameters</u>*:* We derived the values of $\beta_{An}$and β_{Af} used in Eq. 17 and 18 from the weights of the LWS model fitting by rewriting Eq 1 as below:

$$R_{(An,f)pred} = w_{nAn}R_n + w_{fAn}R_f + c \qquad (14a)$$

$$R_{(n,Af)pred} = w_{nAf}R_n + w_{fAf}R_f + c \qquad (14b)$$

w_{nAn}, w_{fAn} and w_{nAf}, w_{fAf} are the weights of near and far components in the two attention conditions, respectively. c >0. We assume that attention to a component of bidirectional stimuli only scales the weight of the attended component (scaled by β_{An} and β_{Af} factors), but not the weight of the other/un-attended component (scaled by a factor of 1).

$$w_{nAn} = w_n * \beta_{An}$$

$$w_{fAn} = w_f * 1$$

$$w_{nAf} = w_n * 1$$

$$w_{fAf} = w_f * \beta_{Af}$$

$$\beta_{An} = \frac{w_{nAn}}{w_{nAf}} \;\; ; \; \beta_{Af} = \frac{w_{fAf}}{w_{fAn}} \qquad (15a; 15b)$$

To evaluate the goodness of fit of a model for the response tuning curve to the bidirectional stimuli, we calculated the percentage of variance (PV) the model accounts for as follows:

$$PV = 100 * (1 - SSE)/SST \qquad (16)$$

where SSE is the sum of squared errors between the model fit and the neuronal data, and SST is the sum of squared differences between the data and the mean of the data.

References

Ban H, Preston TJ, Meeson A, Welchman AE: The integration of motion and disparity cues to depth in dorsal visual cortex. *Nat Neurosci.* 2012, *15:*636-643.

Bao P, Tsao DY: Representation of multiple objects in macaque category-selective areas. *Nat Commun.* 2018, *9:*1774.

Bradley DC, Qian N, Andersen RA: Integration of motion and stereopsis in middle temporal cortical area of macaques. *Nature.* 1995, *373:*609-611.

Bradshaw MF, Rogers BJ: The interaction of binocular disparity and motion parallax in the computation of depth. *Vision Res.* 1996, *36:*3457-3468.

Busse L, Wade AR, Carandini M: Representation of concurrent stimuli by population activity in visual cortex. *Neuron.* 2009, *64:*931-942.

Carandini M, Heeger DJ, Movshon JA: Linearity and normalization in simple cells of the macaque primary visual cortex. *J Neurosci.* 1997, *17:*8621-8644.

Cavanagh P, Caplovitz GP, Lytchenko TK, et al.: The Architecture of Object-Based Attention. *Psychon Bull Rev.* 2023.

Chen G, Lu HD, Roe AW: A map for horizontal disparity in monkey V2. *Neuron.* 2008, *58:*442-450.

Cheng K, Hasegawa T, Saleem KS, Tanaka K: Comparison of neuronal selectivity for stimulus speed, length, and contrast in the prestriate visual cortical areas V4 and MT of the macaque monkey. *J Neurophysiol.* 1994, *71:*2269-2280.

DeAngelis GC, Newsome WT: Organization of disparity-selective neurons in macaque area MT. *J Neurosci.* 1999, *19:*1398-1415.

DeAngelis GC, Uka T: Coding of horizontal disparity and velocity by MT neurons in the alert macaque. *J Neurophysiol.* 2003, *89:*1094-1111.

Desimone R, Duncan J: Neural mechanisms of selective visual attention. *Annual Review of Neuroscience.* 1995, *18:*193-222.

Duncan J: Selective attention and the organization of visual information. *J Exp Psychol Gen.* 1984, *113:*501-517.

Fallah M, Stoner GR, Reynolds JH: Stimulus-specific competitive selection in macaque extrastriate visual area V4. *Proc Natl Acad Sci U S A.* 2007, *104:*4165-4169.

Ferrera VP, Lisberger SG: The effect of a moving distractor on the initiation of smooth-pursuit eye movements. *Vis Neurosci.* 1997, *14:*323-338.

Ghose GM, Maunsell JH: Spatial summation can explain the attentional modulation of neuronal responses to multiple stimuli in area V4. *J Neurosci.* 2008, *28:*5115-5126.

Gonzalez F, Bermudez MA, Vicente AF, Romero MC: Orientation preference and horizontal disparity sensitivity in the monkey visual cortex. *Ophthalmic Physiol Opt.* 2010, *30:*824-833.

Gonzalez F, Perez R, Justo MS, Bermudez MA: Receptive field organization of disparity-sensitive cells in Macaque medial superior temporal cortex. *Eur J Neurosci.* 2001, *14:*167-

173.

Goutcher R: Motion direction influences surface segmentation in stereo transparency. *J Vis.* 2016, *16:*17.

Greenwood JA, Edwards M: Pushing the limits of transparent-motion detection with binocular disparity. *Vision Res.* 2006, *46:*2615-2624.

Heeger DJ: Normalization of cell responses in cat striate cortex. *Vis Neurosci.* 1992, *9:*181-197.

Heuer HW, Britten KH: Contrast dependence of response normalization in area MT of the rhesus macaque. *J Neurophysiol.* 2002, *88:*3398-3408.

Hibbard PB, Bradshaw MF: Does binocular disparity facilitate the detection of transparent motion? *Perception.* 1999, *28:*183-191.

Hinkle DA, Connor CE: Quantitative characterization of disparity tuning in ventral pathway area V4. *J Neurophysiol.* 2005, *94:*2726-2737.

Huang X, Ghimire B, Chakrala AS, Wiesner S: Neural coding of multiple motion speeds in visual cortical area MT. *bioRxiv.* 2023.

Huang X, Wang C, Arseneau B, Yerxa TE, Cooper EA. Natural scene statistics of depth and motion pertinent to figure-ground segregation. *Society for Neuroscience Abstract* 2019.

Kohler PJ, Cottereau BR, Norcia AM: Image Segmentation Based on Relative Motion and Relative Disparity Cues in Topographically Organized Areas of Human Visual Cortex. *Sci Rep.* 2019, *9:*9308.

Kouh M, Poggio T: A canonical neural circuit for cortical nonlinear operations. *Neural Comput.* 2008, *20:*1427-1451.

Krekelberg B, van Wezel RJ: Neural mechanisms of speed perception: transparent motion. *J Neurophysiol.* 2013, *110:*2007-2018.

Lee J, Maunsell JH: A normalization model of attentional modulation of single unit responses. *PLoS One.* 2009, *4:*e4651.

Li X, Basso MA: Competitive stimulus interactions within single response fields of superior colliculus neurons. *J Neurosci.* 2005, *25:*11357-11373.

Luck SJ, Chelazzi L, Hillyard SA, Desimone R: Neural mechanisms of spatial selective attention in areas V1, V2, and V4 of macaque visual cortex. *J Neurophysiol.* 1997, *77:*24-42.

Martinez-Trujillo JC, Treue S: Feature-based attention increases the selectivity of population responses in primate visual cortex. *Curr Biol.* 2004, *14:*744-751.

Maunsell JH, Treue S: Feature-based attention in visual cortex. *Trends Neurosci.* 2006, *29:*317-322.

Maunsell JH, Van Essen DC: Functional properties of neurons in middle temporal visual area of the macaque monkey. I. Selectivity for stimulus direction, speed, and orientation. *J Neurophysiol.* 1983a, *49:*1127-1147.

Maunsell JH, Van Essen DC: Functional properties of neurons in middle temporal visual area of the macaque monkey. II. Binocular interactions and sensitivity to binocular disparity. *J Neurophysiol.* 1983b, *49:*1148-1167.

McDonald JS, Clifford CW, Solomon SS, Chen SC, Solomon SG: Integration and segregation of multiple motion signals by neurons in area MT of primate. *J Neurophysiol.* 2014, *111:*369-378.

Mitchell JF, Stoner GR, Fallah M, Reynolds JH: Attentional selection of superimposed surfaces cannot be explained by modulation of the gain of color channels. *Vision Res.* 2003, *43:*1323-1328.

Mitchell JF, Stoner GR, Reynolds JH: Object-based attention determines dominance in binocular rivalry. *Nature.* 2004, *429:*410-413.

Moran J, Desimone R: Selective attention gates visual processing in the extrastriate cortex. *Science.* 1985, *229:*782-784.

Nawrot M, Blake R: Neural integration of information specifying structure from stereopsis and motion. *Science.* 1989, *244:*716-718.

Ni AM, Maunsell JHR: Neuronal Effects of Spatial and Feature Attention Differ Due to Normalization. *J Neurosci.* 2019, *39:*5493-5505.

Ni AM, Ray S, Maunsell JH: Tuned normalization explains the size of attention modulations. *Neuron.* 2012, *73:*803-813.

Prince SJ, Cumming BG, Parker AJ: Range and mechanism of encoding of horizontal disparity in macaque V1. *J Neurophysiol.* 2002, *87:*209-221.

Qian N, Andersen RA: Transparent motion perception as detection of unbalanced motion signals. II. Physiology. *J Neurosci.* 1994, *14:*7367-7380.

Recanzone GH, Wurtz RH: Effects of attention on MT and MST neuronal activity during pursuit initiation. *J Neurophysiol.* 2000, *83:*777-790.

Reynolds JH, Chelazzi L, Desimone R: Competitive mechanisms subserve attention in macaque areas V2 and V4. *J Neurosci.* 1999, *19:*1736-1753.

Reynolds JH, Heeger DJ: The normalization model of attention. *Neuron.* 2009, *61:*168-185.

Roelfsema PR, Lamme VA, Spekreijse H: Object-based attention in the primary visual cortex of the macaque monkey. *Nature.* 1998, *395:*376-381.

Ruff DA, Born RT: Feature attention for binocular disparity in primate area MT depends on tuning strength. *J Neurophysiol.* 2015, *113:*1545-1555.

Rust NC, Mante V, Simoncelli EP, Movshon JA: How MT cells analyze the motion of visual patterns. *Nat Neurosci.* 2006, *9:*1421-1431.

Samonds JM, Potetz BR, Lee TS: Relative luminance and binocular disparity preferences are correlated in macaque primary visual cortex, matching natural scene statistics. *Proc Natl Acad Sci U S A.* 2012, *109:*6313-6318.

Sclar G, Maunsell JH, Lennie P: Coding of image contrast in central visual pathways of the macaque monkey. *Vision Res.* 1990, *30:*1-10.

Seidemann E, Newsome WT: Effect of spatial attention on the responses of area MT neurons. *J Neurophysiol.* 1999, *81:*1783-1794.

Simoncelli EP, Heeger DJ: A model of neuronal responses in visual area MT. *Vision Res.* 1998,

*38:*743-761.

Smolyanskaya A, Ruff DA, Born RT: Joint tuning for direction of motion and binocular disparity in macaque MT is largely separable. *J Neurophysiol.* 2013, *110:*2806-2816.

Snowden RJ, Rossiter MC: Stereoscopic depth cues can segment motion information. *Perception.* 1999, *28:*193-201.

Snowden RJ, Treue S, Erickson RG, Andersen RA: The response of area MT and V1 neurons to transparent motion. *J Neurosci.* 1991, *11:*2768-2785.

Tanabe S, Doi T, Umeda K, Fujita I: Disparity-tuning characteristics of neuronal responses to dynamic random-dot stereograms in macaque visual area V4. *J Neurophysiol.* 2005, *94:*2683-2699.

Treue S, Hol K, Rauber HJ: Seeing multiple directions of motion-physiology and psychophysics. *Nat Neurosci.* 2000, *3:*270-276.

Treue S, Martinez Trujillo JC: Feature-based attention influences motion processing gain in macaque visual cortex. *Nature.* 1999, *399:*575-579.

Treue S, Maunsell JH: Attentional modulation of visual motion processing in cortical areas MT and MST. *Nature.* 1996, *382:*539-541.

Valdes-Sosa M, Cobo A, Pinilla T: Transparent motion and object-based attention. *Cognition.* 1998, *66:*B13-B23.

Valdes-Sosa M, Cobo A, Pinilla T: Attention to object files defined by transparent motion. *J Exp Psychol Hum Percept Perform.* 2000, *26:*488-505.

Wallace JM, Mamassian P: The efficiency of speed discrimination for coherent and transparent motion. *Vision Res.* 2003, *43:*2795-2810.

Wallace JM, Mamassian P: The efficiency of depth discrimination for non-transparent and transparent stereoscopic surfaces. *Vision Res.* 2004, *44:*2253-2267.

Wannig A, Rodriguez V, Freiwald WA: Attention to surfaces modulates motion processing in extrastriate area MT. *Neuron.* 2007, *54:*639-651.

Wiesner S, Baumgart IW, Huang X: Spatial Arrangement Drastically Changes the Neural Representation of Multiple Visual Stimuli That Compete in More Than One Feature Domain. *J Neurosci.* 2020, *40:*1834-1848.

Wiesner S, Huang X. Image segmentation and neural representation of multiple spatially-separated stimuli in cortical area MT. *Society for Neuroscience Abstract* 2019.

Xiao J, Huang X: Distributed and Dynamic Neural Encoding of Multiple Motion Directions of Transparently Moving Stimuli in Cortical Area MT. *J Neurosci.* 2015, *35:*16180-16198.

Xiao J, Niu YQ, Wiesner S, Huang X: Normalization of neuronal responses in cortical area MT across signal strengths and motion directions. *J Neurophysiol.* 2014, *112:*1291-1306.

The role of binocular disparity in the neural representation of multiple moving stimuli in the visual cortex

Supplementary material

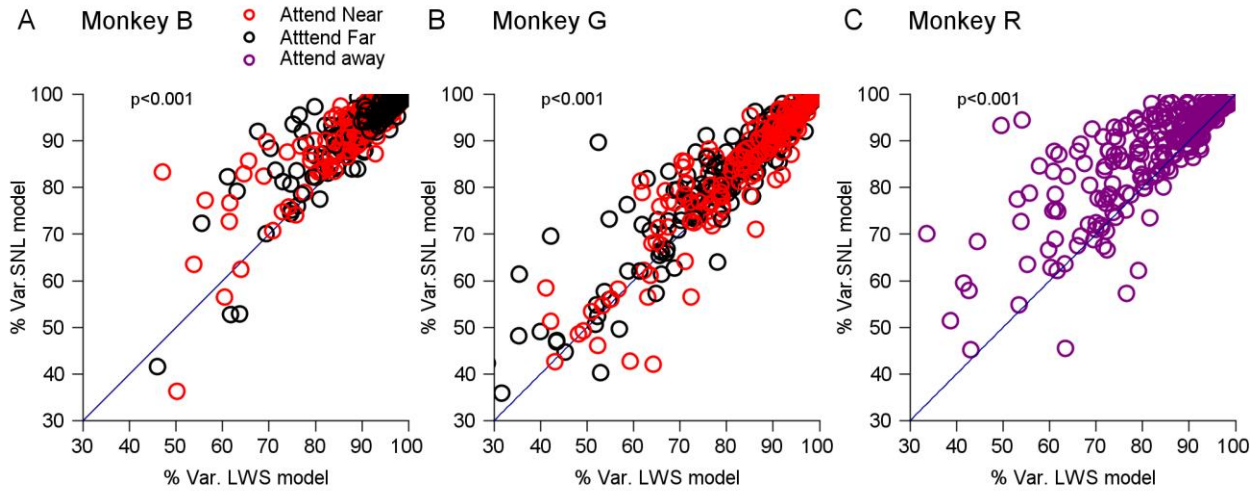

Supplementary Figure 1. Goodness of fits LWS model vs SNL model

A. Comparison of % Var. (percent variance *PV* Eq. 16) of SNL and LWS model fits of monkey B. Red and black dots indicate the fits of bidirectional tuning curves from "Attend Near" and "Attend Far" conditions. **B.** Monkey G. **C.** Monkey R from "Attend Away" paradigm. p values are from one-sided sign rank test. Blue lines indicate x=y line.

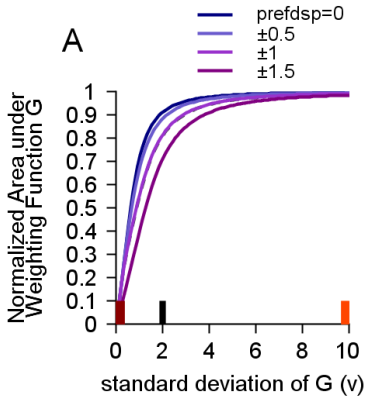

Supplementary Figure 2. Relationship between area under Weighting function ***G*** and standard deviation v

A. Area under Weighting function ***G*** vs standard deviation v in the divisive normalization model (Eq. 6, 7, 9). The different colors represent the different preferred disparity (prefdsp) values of neurons. The brown, black, and orange indicate the v values of Local, Intermediate, and Global pooling strategies shown in Fig 13.